

AD-A129 752

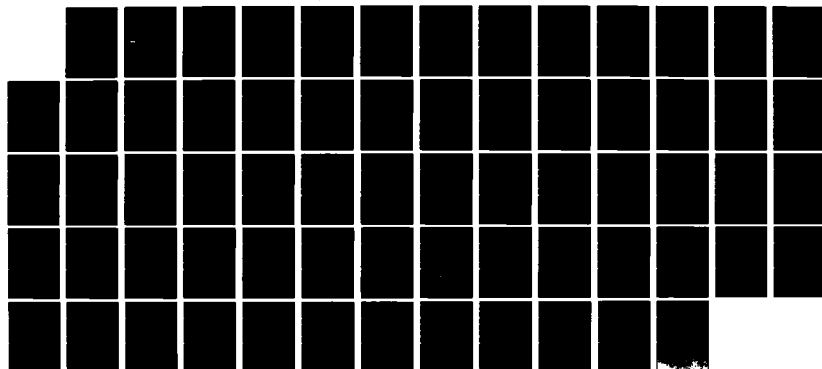
INVESTIGATION OF THE ENDOCHRONIC CONCRETE MODEL(U) NEW
MEXICO ENGINEERING RESEARCH INST ALBUQUERQUE
J W JETER ET AL. MAY 83 AFWL-TR-83-4 F29601-81-C-0013

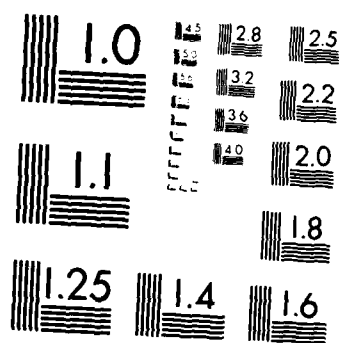
1/1

UNCLASSIFIED

F/G 11/2

NL





MICROCOPY RESOLUTION TEST CHART
NATIONAL BUREAU OF STANDARDS 1963-A

ADA 1297522

INVESTIGATION OF THE ENDOCHRONIC CONCRETE MODEL

J. W. Jeter

J. E. Bean

New Mexico Engineering Research Institute
University of New Mexico
Albuquerque, New Mexico 87131

May 1983

Final Report

Approved for public release; distribution unlimited.

AIR FORCE WEAPONS LABORATORY
Air Force Systems Command
Kirtland Air Force Base, NM 87117

DTIC FILE COPY



This final report was prepared by the New Mexico Engineering Institute Albuquerque, New Mexico, under Contract F29601-81-C-0013, Job Order 88091354 with the Air Force Weapons Laboratory, Kirtland Air Force Base, New Mexico. Rodney G. Galloway (NTES) was the Laboratory Project Officer-in-Charge.

When Government drawings, specifications, or other data are used for any purpose other than in connection with a definitely Government-related procurement, the United States Government incurs no responsibility or any obligation whatsoever. The fact that the Government may have formulated or in any way supplied the said drawings, specifications, or other data, is not to be regarded by implication, or otherwise in any manner construed, as licensing the holder, or any other person or corporation; or as conveying any rights or permission to manufacture, use, or sell any patented invention that may in any way be related thereto.

This report has been authored by a contractor of the United States Government. Accordingly, the United States Government retains a nonexclusive, royalty-free license to publish or reproduce the material contained herein, or allow others to do so, for the United States Government purposes.

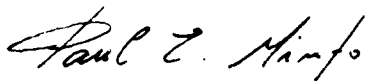
This report has been reviewed by the Public Affairs Office and is releasable to the National Technical Information Services (NTIS). At NTIS, it will be available to the general public, including foreign nations.

If your address has changed, if you wish to be removed from our mailing list, or if your organization no longer employs the addressee, please notify AFWL/NTES, Kirtland AFB, NM 87117 to help us maintain a current mailing list.

This technical report has been reviewed and is approved for publication.



RODNEY G. GALLOWAY
Project Officer



PAUL E. MINTO
Capt, USAF
Chief, Applications branch

FOR THE COMMANDER



JOHN H. STORM
Col, USAF
Chief, Civil Engrg Rsch Division

DO NOT RETURN COPIES OF THIS REPORT UNLESS CONTRACTUAL OBLIGATIONS OR NOTICE ON A SPECIFIC DOCUMENT REQUIRES THAT IT BE RETURNED.

UNCLASSIFIED

SECURITY CLASSIFICATION OF THIS PAGE (When Data Entered)

REPORT DOCUMENTATION PAGE		READ INSTRUCTIONS BEFORE COMPLETING FORM
1. REPORT NUMBER AFWL-TR-83-4	2. GOVT ACCESSION NO. AD A129 752	3. RECIPIENT'S CATALOG NUMBER
4. TITLE (and Subtitle) INVESTIGATION OF THE ENDOCHRONIC CONCRETE MODEL		5. TYPE OF REPORT & PERIOD COVERED Final Report
		6. PERFORMING ORG. REPORT NUMBER
7. AUTHOR(s) J. W. Jeter J. E. Bean		8. CONTRACT OR GRANT NUMBER(s) F29601-81-C-0013
9. PERFORMING ORGANIZATION NAME AND ADDRESS New Mexico Engineering Research Institute University of New Mexico, Box 25, University Station, Albuquerque, New Mexico 87117		10. PROGRAM ELEMENT, PROJECT, TASK AREA & WORK UNIT NUMBERS 62601F/88091354
11. CONTROLLING OFFICE NAME AND ADDRESS Air Force Weapons Laboratory (NTES) Kirtland Air Force Base, NM 87117		12. REPORT DATE May 1983
		13. NUMBER OF PAGES 64
14. MONITORING AGENCY NAME & ADDRESS (if different from Controlling Office)		15. SECURITY CLASS. (of this report) Unclassified
		15a. DECLASSIFICATION DOWNGRADING SCHEDULE
16. DISTRIBUTION STATEMENT (of this Report) Approved for public release; distribution unlimited.		
17. DISTRIBUTION STATEMENT (of the abstract entered in Block 20, if different from Report)		
18. SUPPLEMENTARY NOTES		
19. KEY WORDS (Continue on reverse side if necessary and identify by block number)		
Concrete Constitutive Equations Cyclic Loads Fracturing	Inelastic Action Nonlinear Systems Plasticity Viscoplasticity	Endochronic Theory Strain Rate Effects Path Dependence
20. ABSTRACT (Continue on reverse side if necessary and identify by block number)		
<p>This report describes a continuing evaluation effort on the hysteretic-fracturing endochronic concrete model developed by Bazant and Schieh. The ability of the model to synthesize concrete behavior for a variety of standard and nonstandard load paths is studied through comparisons made with the triaxial test data on plain concrete recently generated at New Mexico State University. The model provided a reasonable match to the experimental data. A Three-dimensional version of the endochronic algorithm was developed. A (over)</p>		

DD FORM 1 JAN 73 1473

EDITION OF 1 NOV 65 IS OBSOLETE

UNCLASSIFIED

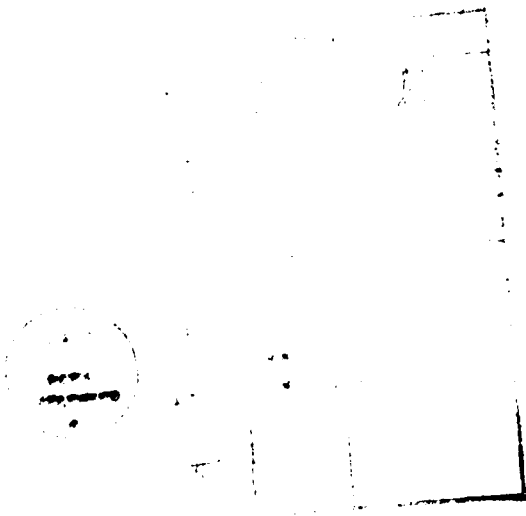
SECURITY CLASSIFICATION OF THIS PAGE (When Data Entered)

UNCLASSIFIED

SECURITY CLASSIFICATION OF THIS PAGE(When Data Entered)

20. ABSTRACT (Continued).

scheme was proposed which would allow for inclusion of high strain rate effects in the model. Simplified versions of the model which would significantly reduce computer storage requirements were devised and investigated.



UNCLASSIFIED

SECURITY CLASSIFICATION OF THIS PAGE(When Data Entered)

CONTENTS

<u>Section</u>		<u>Page</u>
I	INTRODUCTION	5
	Goals Associated with Model Development	5
	Objective and Scope	5
II	REVIEW OF THE ENDOCHRONIC CONCRETE MODEL	7
	Review of the Bazant-Schieh Endochronic Model	7
	Modification to the Bazant-Schieh Model	9
	Review of the Directional Cracking Model	10
III	PATH-DEPENDENT CHARACTERISTICS OF THE ENDOCHRONIC CONCRETE MODEL	13
	Introduction	13
	Comparison with Experimental Data	13
	Comparison with Stress Paths Involving Tension	26
	Summary	28
IV	GENERALIZATION OF THE ENDOCHRONIC ALGORITHM TO THREE DIMENSIONS	33
	Introduction	33
	Determination of Principal Stresses and Directions	33
	Transformation to Principal or Cracked Basis	36
V	HIGH STRAIN RATE EFFECTS IN THE ENDOCHRONIC CONCRETE MODEL	39
	Introduction	39
	Review of Concrete Strain Rate Effects	39
	Endochronic Approach to High Strain Effects in Concrete	40
	Summary	42
VI	REDUCTION OF STORAGE REQUIREMENTS	45
	Introduction	45
	Alternate Schemes for Hysteresis	45
	Evaluation of Alternate Schemes	46
	Summary	53
VII	CONCLUSIONS AND RECOMMENDATIONS	61
	Conclusions	61
	Recommendations	61
	REFERENCES	63

ILLUSTRATIONS

<u>Figure</u>		<u>Page</u>
1	Stress versus strain for a uniaxial stress path	15
2	Stress versus strain for an equal biaxial stress path	15
3	Stress versus strain for a shear superimposed on a hydrostatic state	17
4	Stress versus strain for the proportional stress path $\sigma_2 = 0.5\sigma_1$	17
5	Stress versus strain for the proportional stress path $\sigma_2 = 0.5\sigma_1$ $\sigma_3 = 0.5\sigma_1$	18
6	Stress versus strain for an equal biaxial loading superimposed on a hydrostatic state	18
7	Stress versus strain for a loading consisting of a hydrostatic state followed by a partial hydrostatic unload, and then an equal biaxial loading	19
8	Stress versus strain for a loading consisting of a hydrostatic state followed by a single uniaxial cycle, and then an equal biaxial loading	19
9	Stress versus strain for a loading consisting of a hydrostatic state followed by a uniaxial loading to failure	21
10	Stress versus strain for a loading consisting of a hydrostatic state followed by an equal biaxial cycle and then a uniaxial loading to failure	21
11	Stress versus strain for a loading consisting of a hydrostatic state followed by a partial hydrostatic unload, and then a shear load to failure	23
12	Stress versus strain for a loading consisting of a hydrostatic state followed by a uniaxial loading, and then a change of principal axes followed by a uniaxial loading to failure	24
13	Loading path of Figure 12 in deviatoric stress space	24
14	Stress versus strain for a loading consisting of an equal biaxial loading, and then an equal uniaxial loading in each of the loaded directions, and then an equal biaxial loading to failure	25
15	Stress versus strain for a loading consisting of a hydrostatic state followed by a shear cycle, and then a partial hydrostatic unload, and then an equal biaxial loading to failure	27
16	Stress versus strain for a uniaxial tension loading path	29

ILLUSTRATIONS (Concluded)

<u>Figure</u>		<u>Page</u>
17	Stress versus strain for a shear loading superimposed on a uniaxial loading	29
18	Calculated and experimental failure points for NMSU loading paths	30
19	Flow chart of the directional cracking model	38
20	Effect of k parameter on the response of the endochronic concrete model for constant strain rates.	43
21	Effect of strain rate on concrete strength (from Ref. 11)	44
22	Stress versus strain for uniaxial cyclic compression using the original hydrostatic endochronic algorithm	47
23	Stress versus strain for uniaxial cyclic compression using the endochronic algorithm without hysteretic consideration	48
24	Stress versus strain for uniaxial cyclic compression using the modified hysteretic endochronic algorithm	49
25	Stress versus strain for uniaxial cyclic compression using the endochronic algorithm with elastic cycling	51
26	Stress versus strain for uniaxial compression with a single partial unloading cycle using the uncorrected jump-kinematic hardening representation	52
27	Stress versus strain for uniaxial compression with a single partial unloading cycle using the modified jump-kinematic hardening representation	54
28	Stress versus strain for uniaxial compression with a single partial unloading cycle for the endochronic algorithm without hysteretic considerations	55
29	Stress versus strain for uniaxial compression with a single partial unloading cycle for the endochronic algorithm with elastic cycling	56
30	Stress versus strain for uniaxial compression with multiple cycling using the original endochronic algorithm	57
31	Stress versus strain for uniaxial compression with multiple cycling using the endochronic algorithm without hysteretic considerations	58
32	Stress versus strain for uniaxial compression with multiple cycling using the endochronic algorithm with elastic cycling	59

I. INTRODUCTION

GOALS ASSOCIATED WITH MODEL DEVELOPMENT

Current analysis capabilities for determination of structural response depend greatly on the ability to model the materials involved. The adequacy of future system design and analysis therefore depends on the development of advanced material models for reinforced concrete. The goal of this modeling effort is to provide a more complete understanding of the behavior of concrete and to provide improved capabilities to analytically model the response of reinforced concrete structures to applied loads, including static loads and dynamic blast and shock-induced loads.

OBJECTIVE AND SCOPE

This report describes a continuing evaluation effort on the hysteretic-fracturing endochronic concrete model developed by Bazant and Schieh (Ref. 1). This model is intended to reproduce all significant aspects of the compressive behavior of concrete except strain rate effects. Endochronic models assume that inelastic strain accumulation can be characterized by a scalar parameter called intrinsic time, whose increment is a function of strain increments. In earlier work (Refs. 2 and 3) it was shown that endochronic theory could reproduce aspects of concrete behavior to a degree never before experienced. This model is a refinement of the earlier work, serving to improve on the duplication of observed behavioral features while removing theoretical inconsistencies. Since the endochronic model is assumed to be one for the compressive behavior of concrete only, it was meshed with a directional cracking tension model to provide a complete depiction of concrete behavior.

The objective of this study is an evaluation and development of the hysteretic-fracturing endochronic model as a viable tool for the analysis of concrete structures. The ability of the model to synthesize concrete behavior for a variety of standard and nonstandard load paths is studied through comparisons made with the triaxial test data on plain concrete recently generated at New Mexico State University. This comparison necessitated the investigation of various parameter adjustment techniques for fitting the model to concretes outside the range for which the model was calibrated. The original

algorithm, which was devised to operate in a two-dimensional finite element structural analysis program, is generalized to three dimensions in this effort in anticipation of its insertion into a more general code.

Explosively loaded systems respond with high strain rates and it is known that concrete is a strain-rate-sensitive material. Current concrete models do not attempt to account for this effect. Although strain rate effects are not included in the endochronic concrete model, the intrinsic time term provides an attractive avenue for the incorporation of such effects. Possible approaches to a strain rate dependency for the model are explored.

One aspect of the endochronic concrete algorithm which is often cited as a major disadvantage is the large number of parameters which must be stored for each element for each increment of a finite element analysis. It is important to note that constitutive relations which attempt to provide a realistic depiction of hysteresis require a large number of storage parameters, so comparisons between the endochronic model and other models which omit hysteresis are inappropriate. It is apparent, however, that the number of parameters associated with the model must be reduced if the model is to be suitable for practical application. In this study, modification of the hysteresis portion of the algorithm is considered as a possible approach for reduction of the number of required element storage parameters.

II. REVIEW OF THE ENDOCHRONIC CONCRETE MODEL

REVIEW OF THE BAZANT-SCHIEH ENDOCHRONIC MODEL

The endochronic model utilized in this analysis consists of two parts: a directional cracking model used to describe tensile behavior, and a modified version of the Bazant-Schieh hysteretic-fracturing endochronic model used to describe compressive behavior. The Bazant-Schieh model was intended to serve as a refinement of the endochronic concrete model developed in an earlier work. The primary improvements to the previous theory involve (1) separate considerations of inelastic strains related to plastic slip of the micro-cracked material and inelastic strains related to strength and rigidity degradation due to microcracking, (2) a more detailed modeling of inelastic volumetric behavior, and (3) institution of a load-unload criterion along with jump-kinematic hardening to better match hysteresis and ensure energy dissipation under cyclic loading.

The intrinsic time parameters used in this model are defined primarily in terms of the deviatoric strain path length, whose increment is

$$d\zeta = \sqrt{\frac{1}{2} de_{km} de_{km}}$$

where

ζ is the deviatoric strain path length

de_{km} is the deviator of the strain tensor

A separate intrinsic time parameter is used for plastic and fracturing deviatoric inelastic strains, so that

$$de_{ij}^{pl} = \frac{S_{ij}^*}{2G} d\zeta \quad (1)$$

and

$$de_{ij}^{fr} = e_{ij}^* d\kappa \quad (2)$$

where

de_{ij}^{pl} , de_{ij}^{fr} are, respectively, the plastic and fracturing inelastic deviatoric strain increments

G is the elastic shear modulus

$$S_{ij}^* = S_{ij} - \alpha_{ij}$$

S_{ij} is the deviatoric stress

$$e_{ij}^* = e_{ij} - \alpha_{ij}'$$

e_{ij} is the deviatoric strain

α_{ij} , α_{ij}' are jump-kinematic hardening parameters

$$d\xi = cF_1 d\xi \text{ (plastic intrinsic time increment)} \quad (3)$$

$$d\kappa = cF_2 d\xi \text{ (fracture intrinsic time increment)} \quad (4)$$

c is a coefficient defining the loading condition

F_1 and F_2 are invariant functions of stress, strain, and ξ

The particular forms of F_1 and F_2 are determined empirically. Expressions similar to Equations 1 and 2 are developed for the dilatational and shear compaction aspects of inelastic volumetric behavior. However, inelastic volumetric behavior due to pore crushing is related to the volumetric strain path length rather than deviatoric strain path length. The volumetric strain path length is defined as

$$d\xi' = \left| d\epsilon_{kk} \right|$$

The earlier endochronic model did not accurately reproduce the hysteretic behavior which occurred during unload-reload cycles and, in fact, violated Drucker's stability postulate. Rectifying these problems required the institution of a loading-unloading criterion with appropriate adjustments for these situations. Separate criteria were suggested for deviatoric and volumetric behavior based, respectively, on deviatoric and volumetric work. Adjustments to unload-reload cycles are then partially made by selecting appropriate values of the constant parameter, c , in Equations 3 and 4, along with a similar parameter involved in the pore crushing contribution to the inelastic volumetric strains. In addition, jump-kinematic hardening is included to complete the unload-reload model.

MODIFICATIONS TO THE BAZANT-SCHIEH MODEL

The parameters defining functions F_1 and F_2 in Equations 3 and 4 and similar functions for inelastic volumetric behavior were determined by fitting data to a form arrived at from a combination of physical reasoning and experience. The resulting expressions are relatively complicated, and are not unique--i.e., variations of the form and parameters in the functions could produce equally satisfactory fits to the experimental data. In this study an algorithm for the endochronic theory was developed and encoded to facilitate the investigation of the model. A slight variation of the form of function F_2 was necessary to produce a satisfactory fit to experimental data. The resulting model produced results which differed slightly from those of Reference 1.

Some questions arose concerning the jump-kinematic hardening associated with the model. The inelastic deviatoric strains are calculated by the equations

$$de_{ij}^{pl} = \frac{s_{ij} - \alpha_{ij}}{2G} cF_1 d\xi \quad (5)$$

and

$$de_{ij}^{fr} = (e_{ij} - \alpha_{ij}^!) cF_2 d\xi \quad (6)$$

as described previously. At the onset of unloading and reloading, the α terms and the c term change values, based on a deviatoric work criterion

$$\begin{aligned} dW > 0, W = W_0 &: \text{virgin loading ; } c = 1 \\ dW < 0 &: \text{unloading ; } c = c_u = 0.6 ; \alpha_{ij} = S_{ij}, \alpha_{ij}^! = e_{ij} \text{ (unloading)} \\ dW > 0, W < W_0 &: \text{reloading ; } c = c_r = 0.8 ; \alpha_{ij} = s_{ij}, \\ &\alpha_{ij}^! = e_{ij} \text{ (reloading)} \end{aligned}$$

where

$$dW = s_{km} de_{km}$$

W_0 = maximum value of W yet achieved

A similar formulation is used for volumetric unloading and reloading.

Although this approach works quite well when the material is completely unloaded, it appears to break down under a partial unloading. Since the α and α' values in Equations 5 and 6 are defined at the start of unloading and at the start of reloading, but not at renewed virgin loading, artificial hardening is produced whenever the material is not subject to a significant unloading. Accounting for this artificial hardening was apparently a consideration in the application of jump-kinematic hardening to the plastic fracturing concrete theory of Bazant and Kim (Ref. 3). A remedy that appears to work for this situation is to reset the α_{ij} and α'_{ij} terms to zero when the virgin loading path is renewed. A similar adjustment is made for volumetric behavior. The resulting depiction of the concrete behavior is consistent with that observed experimentally.

REVIEW OF THE DIRECTIONAL CRACKING MODEL

The endochronic concrete model was designed to reproduce characteristic compressive behavior of concrete. Tensile (cracking) behavior must be modeled separately if the material model is to be considered for general finite element applications. A proper cracking model works with principal stresses, can accommodate compressive loading of the crack, produces gradual cracking, and allows for a partial resistance to shear remaining on the crack plane.

A suitable model was obtained by modifying the cracking approach used for an earlier endochronic formulation. This model is built around the concept that cracking produces a free surface so that, for instance, a plane stress problem is reduced to a uniaxial stress formulation through the formation of a crack plane normal to the plane of stress. Strains perceived by the material in the direction normal to the crack are not the strains defined by nodal point motion in a finite element program, but instead are dependent on the material behavior in the direction parallel to the crack. This distinction is crucial for continued proper compressive modeling using the

endochronic model. Crack closure is then defined as occurring when the strain perceived by the material becomes as large (compressively) as strains defined by node point motion.

Instantaneous crack formation for an element in a finite element program leads to a phenomenon known as crack shock, which is a misrepresentation of the material behavior due to the inability of the finite element program to properly handle discontinuous behavior. Crack shock can be avoided by allowing the crack plane to develop into a free surface gradually, rather than instantaneously. This is done by gradually dropping the tensile stress down to zero. The transition condition is similar to the free surface condition, except the stress on the crack surface has some specified value other than zero.

The principal modifications made to the earlier cracking model involved introduction of a principal stress formulation and inclusion of a partial resistance to shear on the crack plane. The initial crack check is made by considering stresses in the principal directions. It is known that some reduced shear resistance exists on a rough crack surface. However, retention of shear resistance on crack faces, along with the assumption that cracks occur on principal planes, implies a second crack need not be perpendicular to the first crack. A model which accounts for this behavior would be quite complicated. For the sake of simplicity, it was assumed that a second crack be normal to the first crack. This tensile model produced satisfactory results for test problems and direct applications.

III. PATH-DEPENDENT CHARACTERISTICS OF THE ENDOCHRONIC CONCRETE MODEL

INTRODUCTION

Path dependence is produced in the endochronic model through the definition of the intrinsic time parameters in terms of the strain path length. Whether or not the intrinsic time term accurately models damage accumulation during the loading process must be determined through a consideration of experimental data.

In an earlier phase of this effort (Ref. 4), a number of stress paths were considered to determine what stress path effects would be predicted by the model and to determine whether some failure surface could be associated with the failure conditions predicted by the theory. This study revealed that (1) the model implies a failure surface in the deviatoric plane which is consistent in form with that observed experimentally, and (2) the nature of the endochronic model is to produce failure dependence on the stress path, other than what would be predicted by a failure surface.

The monotonically increasing aspect of the intrinsic time term in endochronic theory would cause it to produce inelastic strain increments for all deviatoric strain increments, including loading tangent to what could be considered the failure surface. The resulting predicted behavior would be somewhat softer than observed concrete behavior and considerably softer than the elastic behavior predicted by a classical plasticity approach to inelastic behavior (Ref. 5). This indicates that the endochronic theory is more conservative than classical plasticity in its depiction of loading to the side.

COMPARISON WITH EXPERIMENTAL DATA

Calibration of model--In this portion of the report, comparisons are made of predictions by the endochronic concrete model for failure conditions and stress path dependence with triaxial data developed recently (Ref. 6). The test program at New Mexico State University (NMSU) was intended to provide information on hardening, limit surfaces, path dependency, and the nature of inelastic deformation in general. A set of standard compressive stress paths was run using cubical specimens, followed by a series of nonstandard stress paths intended to indicate stress path dependency.

The endochronic concrete model can be adapted to many concretes simply by applying the appropriate uniaxial cylinder compressive strength (f_c'). However, this method was unsatisfactory for the NMSU concrete, which had a relatively low strength (25.5 MPa) in comparison to the concretes considered for determination of the internal parameters for the endochronic model. Consequently, an approach recommended by the authors of the theory was used to calibrate the model. After some preliminary runs to study the effect of selected internal parameters on the calculated response, adjustments were made to produce as good a fit as possible to the uniaxial, biaxial, and triaxial test data. The adjusted parameters were then used in the model for the duplication of the other stress paths considered in the test series. Matchups to uniaxial and biaxial behavior are shown in Figures 1 and 2 respectively.

Several comments must be made concerning the adjustment of parameters for materials other than those to which the model had originally been calibrated. Uniaxial compressive strength alone does not provide a complete description of a concrete; other factors such as water content can cause significant variations in behavior. The concrete used in the NMSU test series displayed some features that are dissimilar to those of the concretes used to define the original parameters. For instance, shear enhanced compaction was noticeably reduced, while dilatation was observed to a higher degree. Also, the uniaxial strengths of cubical specimens are commonly lower than those of cylindrical specimens. Because parameter definition in the model is based primarily on specimen behavior that is similar to the behavior of cylinders, the uniaxial strength of cylindrical specimens was used in the calibration. Finally, because the parameters were adjusted by trial and error, the number of parameters varied was kept to a minimum. The model may be more sensitive to some parameters than to others; adjustments of this type may therefore have undesirable ramifications for load paths other than those matched. More recently a curve-fitter program has been used for these adjustments. This program allows a larger number of parameters to be considered.

Comparison of stress-strain relations--Predictions based on the endochronic model were compared to the experimental data from two perspectives: (1) stress-strain plots were used to illustrate the nature of the inelastic deformation produced by the model, and (2) the predicted and measured failure surfaces were evaluated. Because features evident in some stress-strain plots

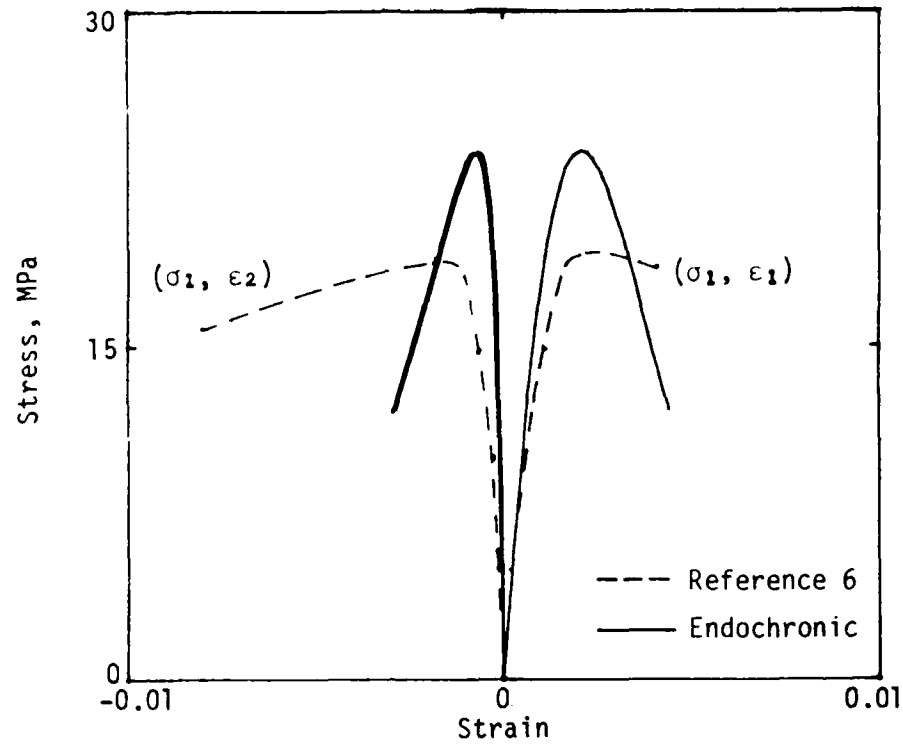


Figure 1. Stress versus strain for a uniaxial stress path.

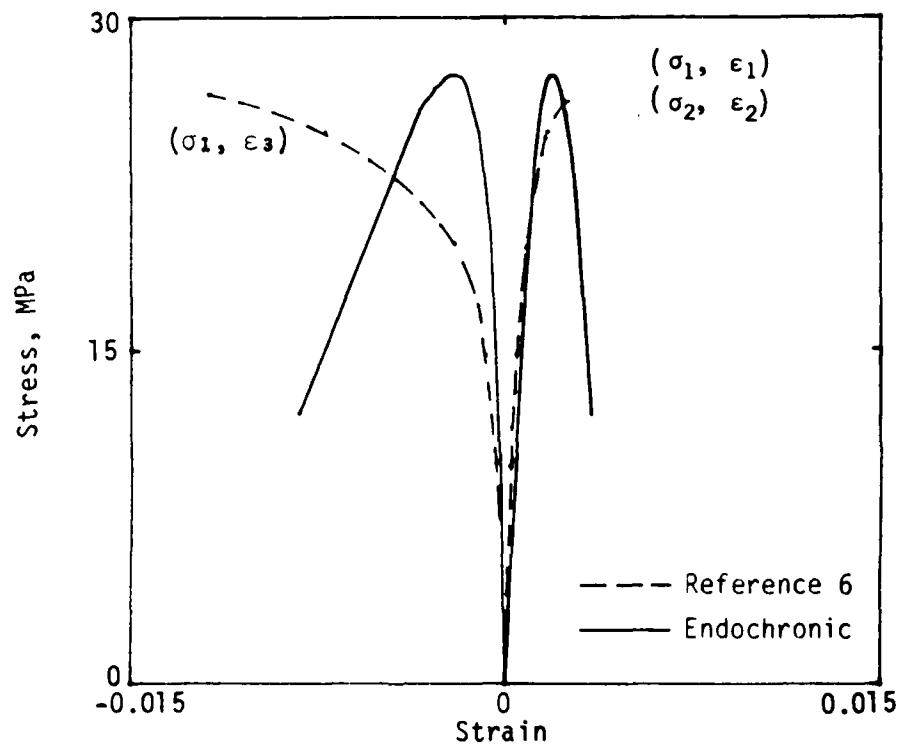


Figure 2. Stress versus strain for an equal biaxial stress path.

are duplicated in others, not all the plots from the stress paths considered are displayed.

Calculated and experimental data are compared in Figure 3 for a loading in which pure shear is superimposed on a hydrostatic loading. Agreement is generally good, although the model somewhat underpredicts inelastic behavior for the unloaded and neutrally loaded directions.

A biaxial stress state with a stress increment in the second principal direction that is one-half that in the first principal direction is shown in Figure 4. The loading in Figure 4 is repeated in the data shown in Figure 5, with the addition that the loading in the third principal direction is equal to one-tenth the loading in the first principal direction. The strength enhancement due to this relatively small confinement effect is visible in both the calculated and the experimental data. The higher stiffness observed in the calculated data may be related to the use of third stress invariant terms within the model for adjusting to triaxial loadings. It is possible that these terms overadjust for cases close to a biaxial condition because similar difficulties were not apparent for more balanced triaxial loadings. The parameter-adjustment technique used in this part of the study would exaggerate this effect.

Three load paths were considered which were variations of the biaxial loading state shown in Figure 2. Figure 6 displays the behavior resulting from a loading path consisting of a hydrostatic load to $0.1 f'_c$ followed by an equal biaxial load. The strength enhancement produced by this relatively small amount of confinement can be seen by comparison with Figure 2 and is suitably depicted by the model.

A cycle is added to the hydrostatic loading for the behavior depicted in Figure 7. A slight hardening is evident in both the experimental and the calculated data as a result of the cyclic loading.

The behavior displayed in Figure 8 is the result of a loading path consisting of a hydrostatic load to $0.1 f'_c$ followed by a uniaxial load-unload

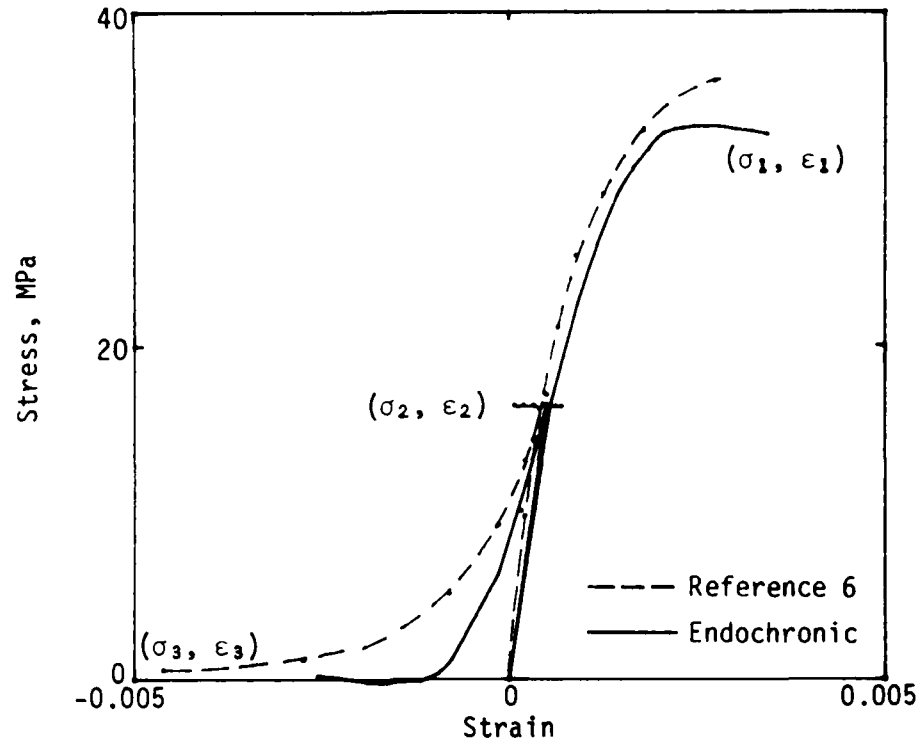


Figure 3. Stress versus strain for a shear superimposed on a hydrostatic state.

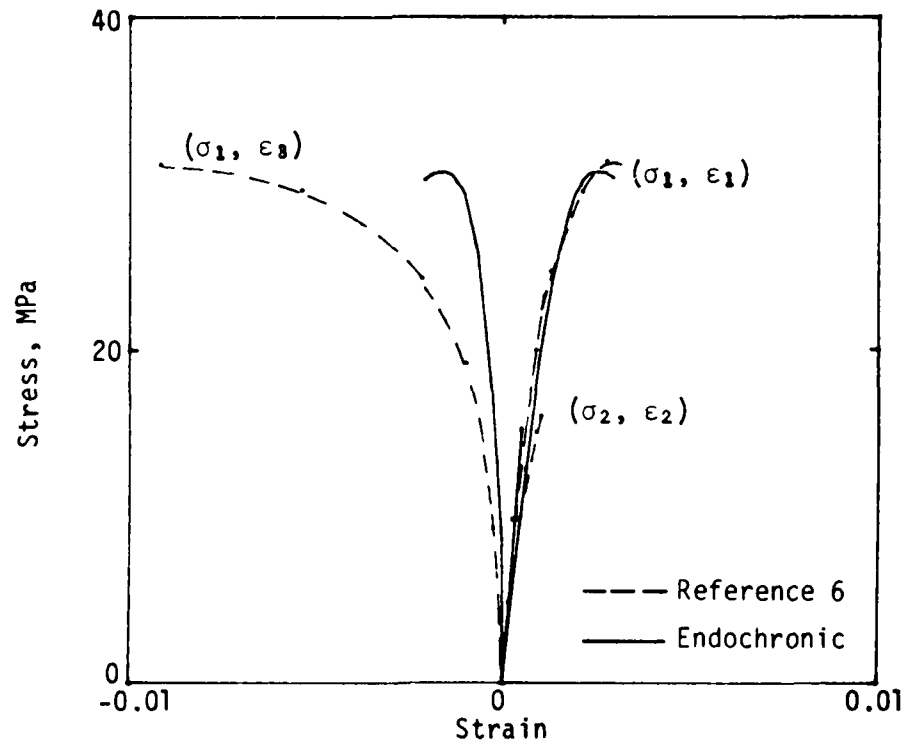


Figure 4. Stress versus strain for the proportional stress path $\sigma_2 = 0.5\sigma_1$.

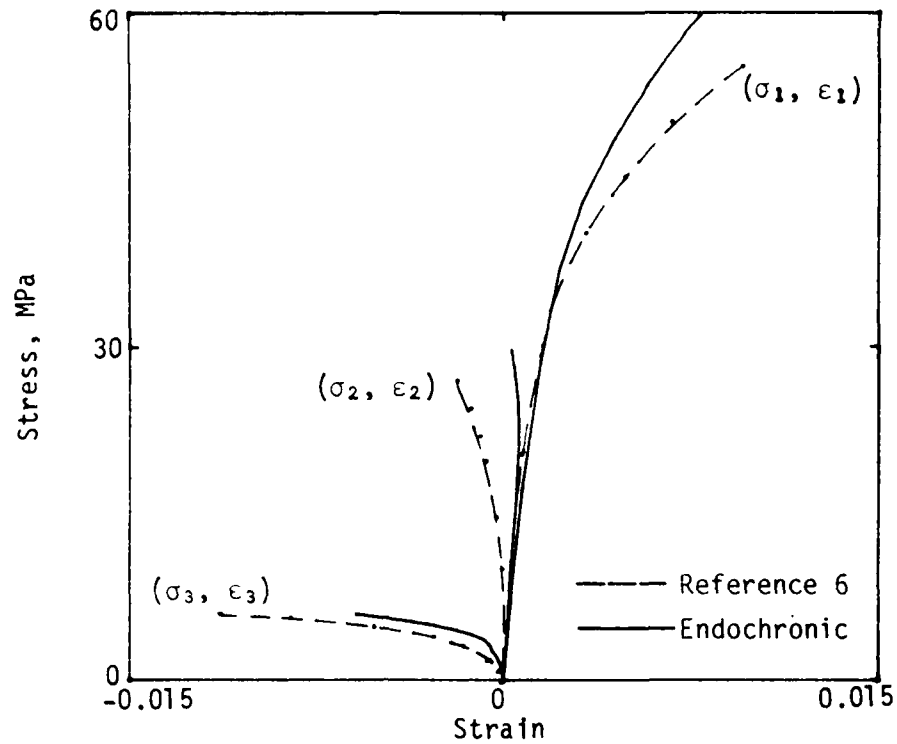


Figure 5. Stress versus strain for the proportional stress path $\sigma_2 = 0.5\sigma_1$, $\sigma_3 = 0.1\sigma_1$.

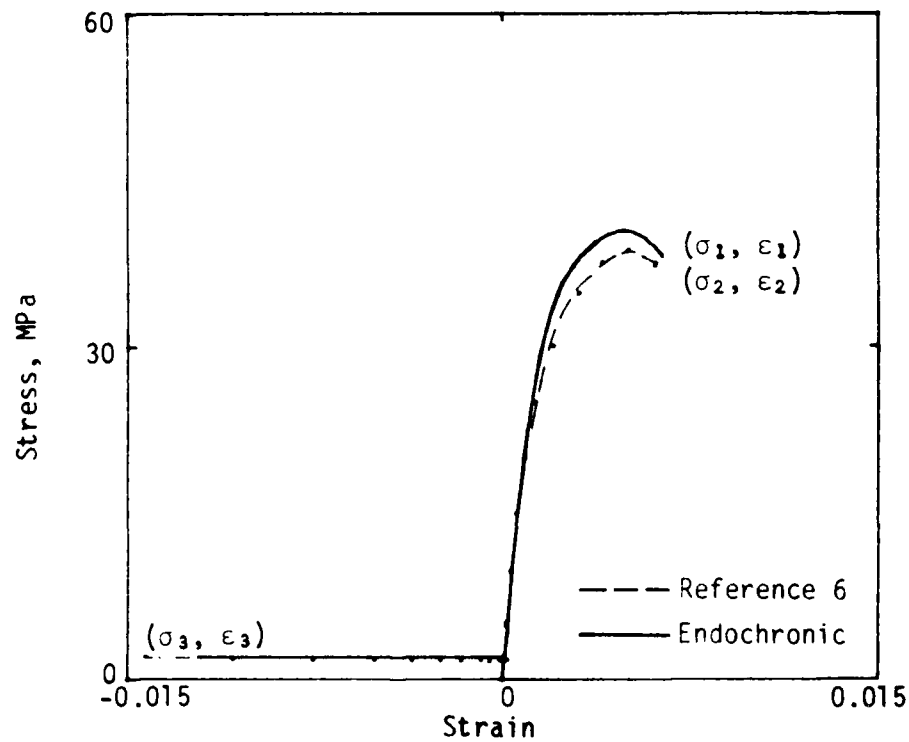


Figure 6. Stress versus strain for an equal biaxial loading superimposed on a hydrostatic state.

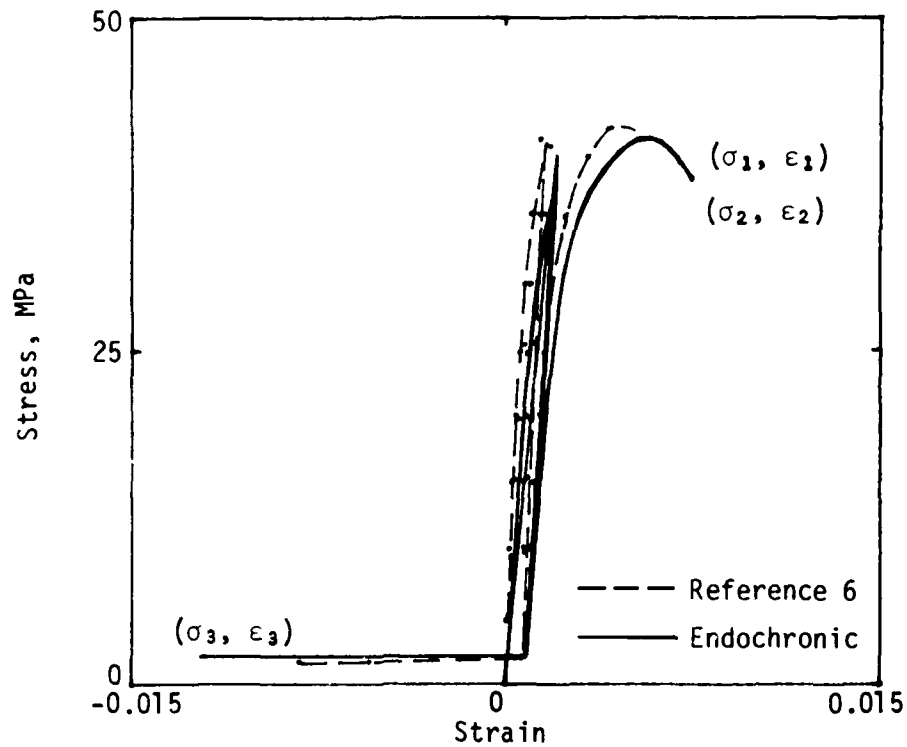


Figure 7. Stress versus strain for a loading consisting of a hydrostatic state followed by a partial hydrostatic unload, and then an equal biaxial loading.

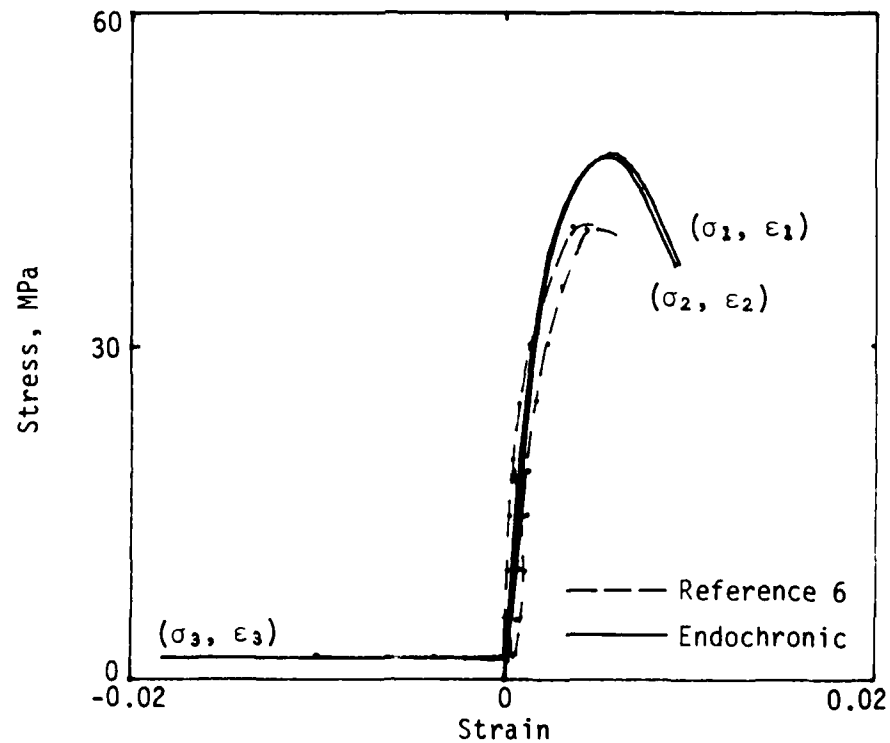


Figure 8. Stress versus strain for a loading consisting of a hydrostatic state followed by a single uniaxial cycle, and then an equal biaxial loading.

cycle and then an equal biaxial loading to failure. The general match to the experimental data is good but the model does not produce the amount of hysteresis found in the experimental data. It is convenient to compare the behavior shown in Figure 8 with that shown in Figure 6, where the results of a similar loading, but with the cycle omitted, are displayed. An apparent increase in strength is seen in the experimental data for the load that includes cycling. This behavior is exaggerated in the model. A possible explanation relates to the approach used to produce hysteresis in the model. When deviatoric unloading begins, the value of the deviatoric strain path length is stored. The deviatoric strain path length is reset to this value when the unload-reload cycle ends, as defined by the restoration of the deviatoric strain energy lost during unloading. (This adjustment is necessary to prevent an exaggeration of hardening in the model due to accumulation of the deviatoric strain path length during cyclic loading.) It is suspected that the change in the nature of the loading causes the deviatoric strain path length to be reset prematurely, which produces higher effective values for the path length than is appropriate and leads to an overly stiff behavior for the model. This hypothesis obtains credence from the behavior shown in Figure 7, where a hydrostatic cycle is substituted for the uniaxial cycle. No excessive strength enhancement occurs for the model in this case because the hydrostatic cycle does not produce a deviatoric strain path length.

Similar comparisons were made for combinations of hydrostatic and uniaxial loads. In Figure 9, behavior is depicted for a loading path consisting of a hydrostatic load to $0.1 f'_c$, followed by a uniaxial loading to failure. Comparison with Figure 1 demonstrates the strength enhancement due to confinement present in both the experimental and calculated data. The model is seen to significantly underpredict the strength of the material under these conditions. This behavior is apparently related to the sensitivity of the model to the invariant terms discussed previously, since the phenomenon was not observed in the calibration triaxial test where the initial hydrostatic load was about $0.4 f'_c$. Figure 10 shows the behavior for a similar loading, but an equal biaxial loading cycle is interjected between the hydrostatic

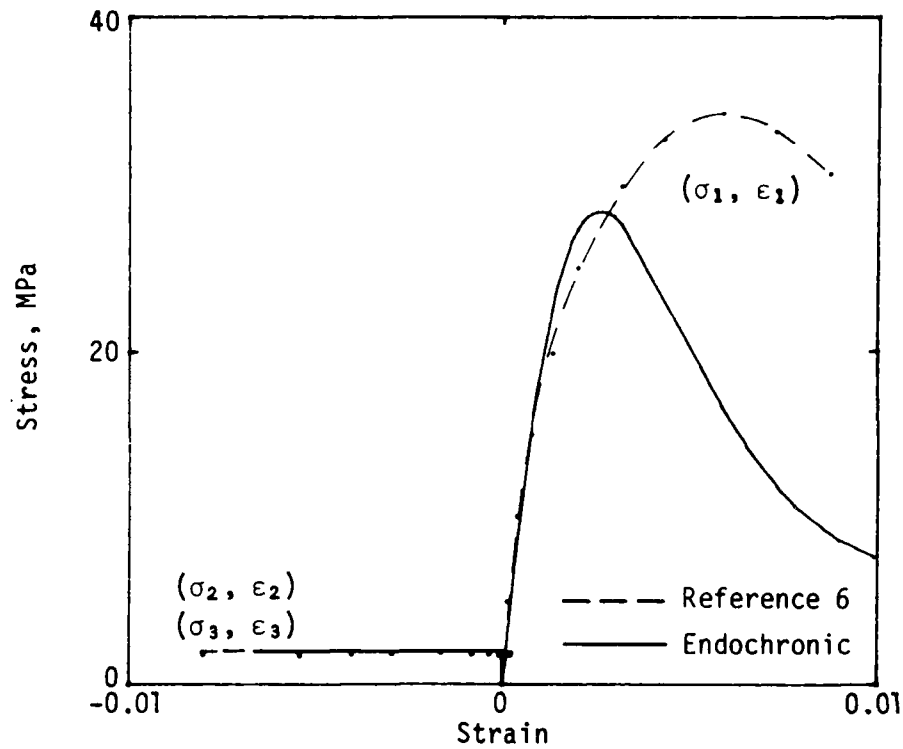


Figure 9. Stress versus strain for a loading consisting of a hydrostatic state followed by a uniaxial loading to failure.

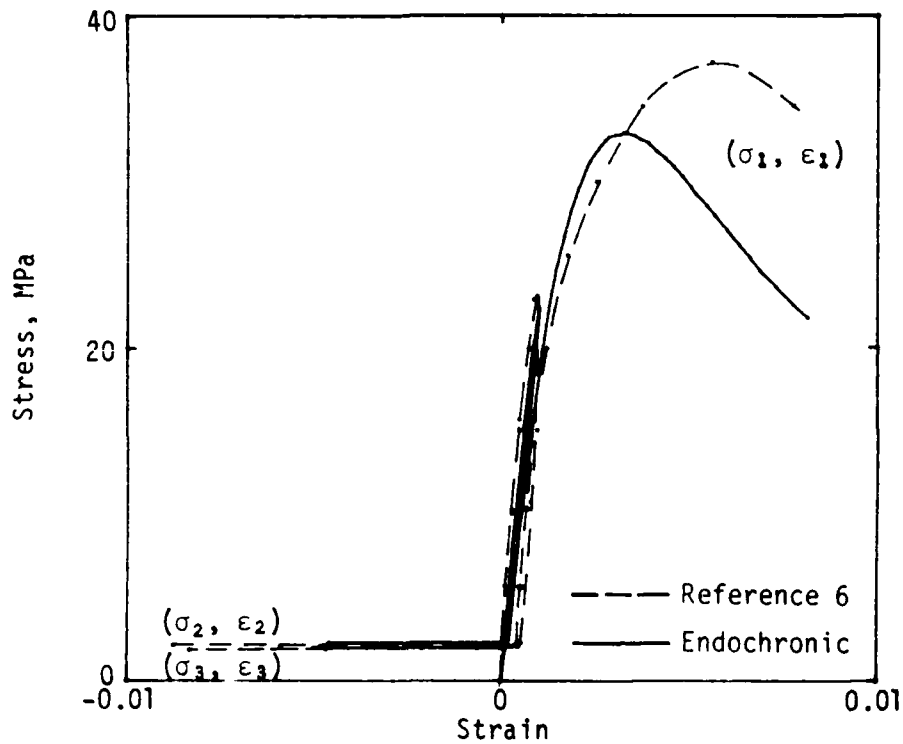


Figure 10. Stress versus strain for a loading consisting of a hydrostatic state followed by an equal biaxial cycle, and then a uniaxial loading to failure.

and uniaxial loadings. This cycle is seen to provide a strength enhancement for both the experimental and calculated data, but the calculated data underpredicts the experimental data to approximately the same degree as seen earlier.

Results from a loading path consisting of a hydrostatic load-partial hydrostatic unload, and then a pure shear load to failure are depicted in Figure 11. Comparison with Figure 3 which depicts the same loading without the hydrostatic cycle reinforces the conclusion previously drawn that hydrostatic cycling in this load range has little influence on material behavior.

The last of the more complicated compressive loading paths to be discussed provide some insight into path-dependent characteristics of the material behavior. Figure 12 displays results for a loading path consisting of a hydrostatic load to $0.1 f'_c$, followed by a uniaxial loading to $0.85 f'_c$, followed by a shear load until the stress condition in the direction of the uniaxial load is switched with that of one of the other loaded directions, followed by a uniaxial load to failure. This rather intricate loading path involves a 120-deg excursion in the deviatoric plane, as shown by path A in Figure 13. Such a loading path would not produce significant inelastic behavior for a material which followed a classical plasticity law. Figure 9, which depicts a similar loading path, but with no excursion, provides a convenient datum. It can be seen that while the excursion results in a slight reduction in the strength for the experimental data, a significant hardening occurs for the calculated data. Such behavior is difficult to interpret, but appears to be related to the discontinuous behavior which can result from the hysteresis portion of the model. The deviatoric strain path length upon which inelastic behavior is based is redefined if an unloading cycle occurs, so loading paths (such as this one) which are very close to a neutral loading can produce ambiguous results.

Figure 14 depicts a loading path consisting of an equal biaxial load to $0.1 f'_c$ followed by a uniaxial load to $0.75 f'_c$, and then a uniaxial load in the second direction to $0.75 f'_c$, followed by a biaxial load to failure. This loading path examines the effect of a loading which roughly parallels the failure line in a $\sqrt{J_2} - I_1$ invariant space. A classical plasticity

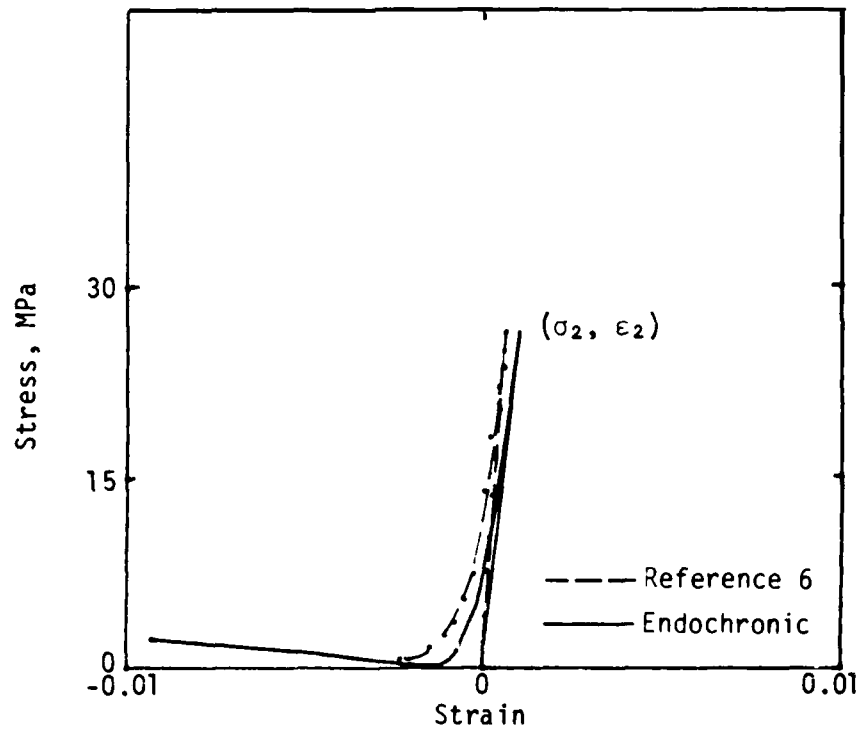
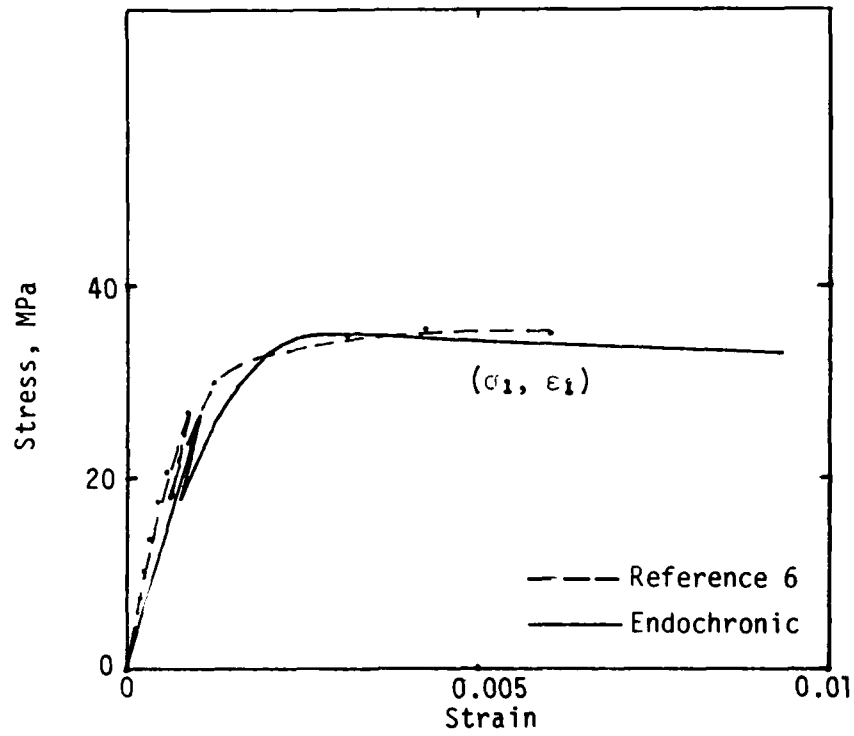


Figure 11. Stress versus strain for a loading consisting of a hydrostatic state followed by a partial hydrostatic unload, and then a shear load to failure.

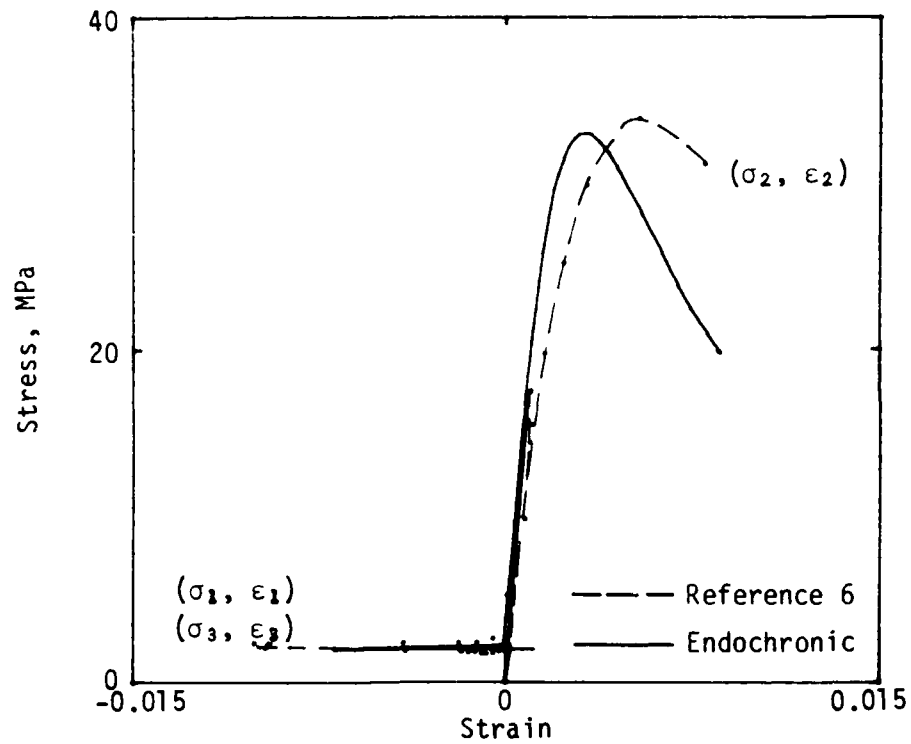


Figure 12. Stress versus strain for a loading consisting of a hydrostatic state followed by a uniaxial loading, and then a change of principal axes followed by a uniaxial load to failure.

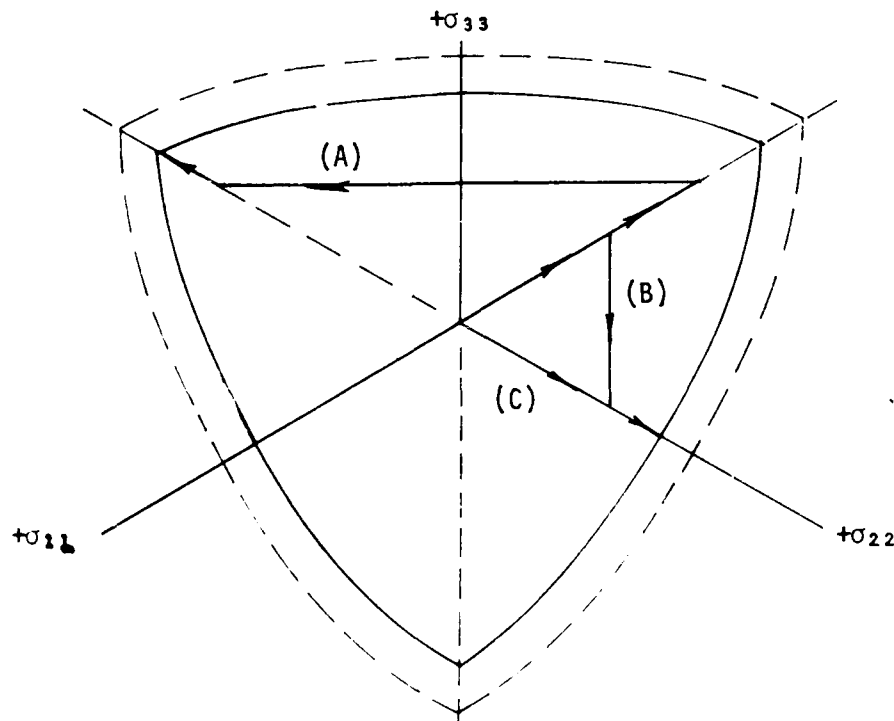


Figure 13. Loading path of Figure 12 in deviatoric stress space (tension positive).

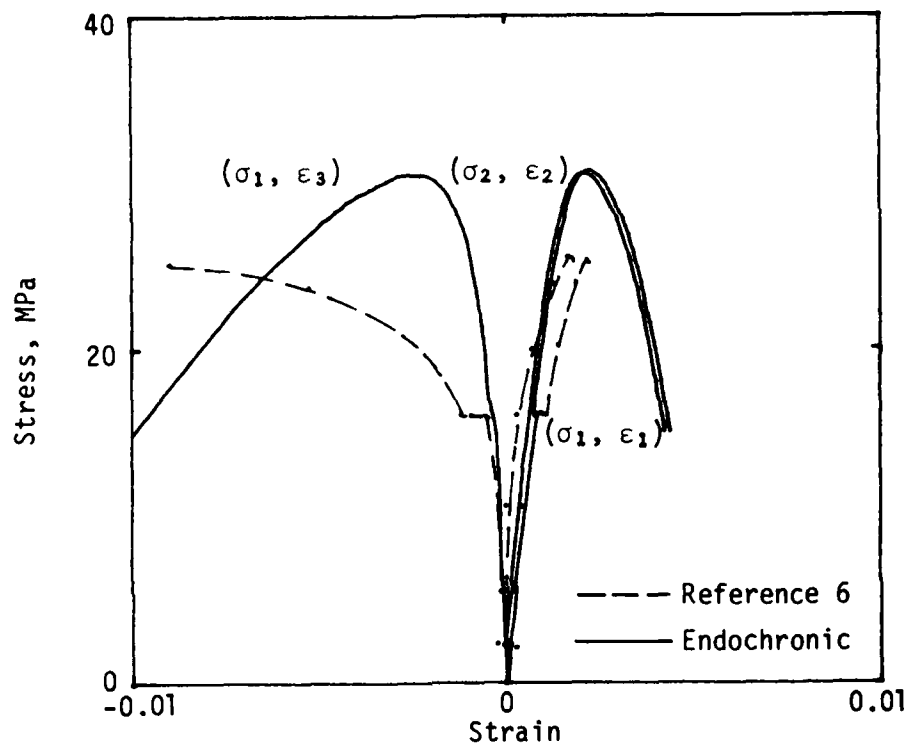


Figure 14. Stress versus strain for a loading consisting of an equal biaxial loading, and then an equal uniaxial loading in each of the loaded directions, and then an equal biaxial loading to failure.

approach would be expected to display little inelastic behavior. A convenient loading path for comparison is shown in Figure 2 which displays an equal biaxial loading. The two paths are depicted in deviatoric space as paths B and C, respectively, in Figure 9. A slight reduction in strength is seen for the experimental data, but a strength increase is predicted by the theory. It is expected that the increased deviatoric strain path length artificially hardens the calculated behavior depiction for the more complicated path. Apparently the presence of inelastic behavior for such paths is countered in the endochronic theory by the hardening effect produced by the longer deviatoric strain path.

In Figure 15, the following loading path is depicted: a hydrostatic loading to $2 f'_c$; then a shear cycle of $\Delta\sigma_1 = \Delta\sigma_2 = f'_c$; then a hydrostatic unload to $0.1 f'_c$ followed by an equal biaxial loading to failure. The three specimens used for this loading path showed widely varying results, possibly because of the difficulty involved in following a prescribed loading path at high stresses. Comparison with Figure 6, which shows the results of a hydrostatic loading to $0.1 f'_c$ followed by an equal biaxial loading, indicates a slight strength gain for the experimental data. The model produces an exaggerated strength gain, probably as a result of the accumulation of the deviatoric strain path length. Otherwise, the model produces results within the spread of the experimental data. The kinks which occur in the calculated results are due to the beginning or ending of volumetric or deviatoric inelastic behavior.

COMPARISON WITH STRESS PATHS INVOLVING TENSION

Loading paths involving tension were also included in the New Mexico State University study. Although the results of these tests are useful for the evaluation of the total concrete model, the tensile cracking model dominates behavior rather than the endochronic (compressive) model. It is important to note that the stress levels and strain levels reached in these tests are quite low. This causes a magnification of the influence of procedure-

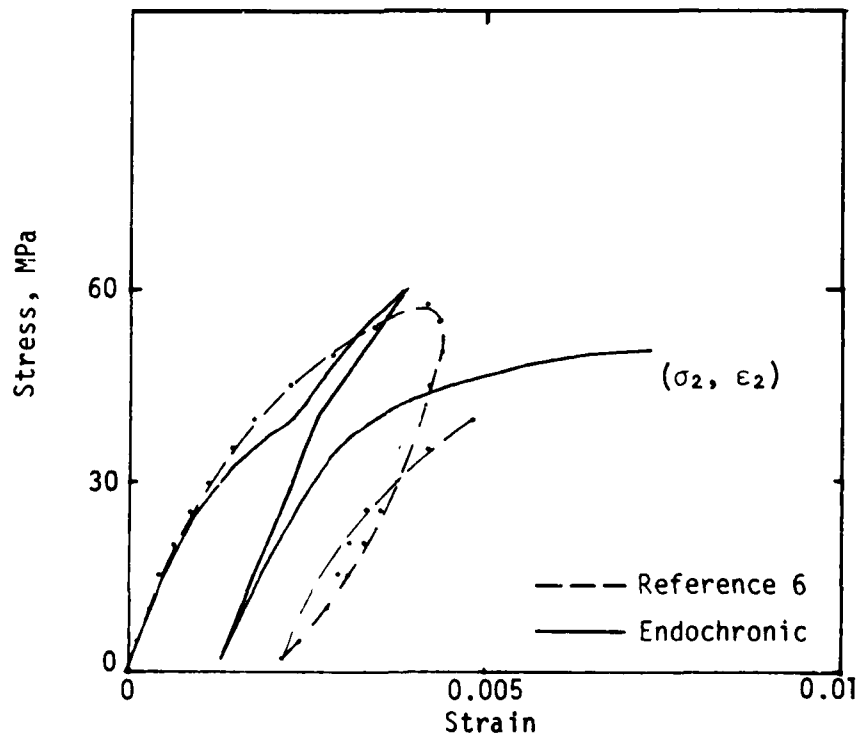
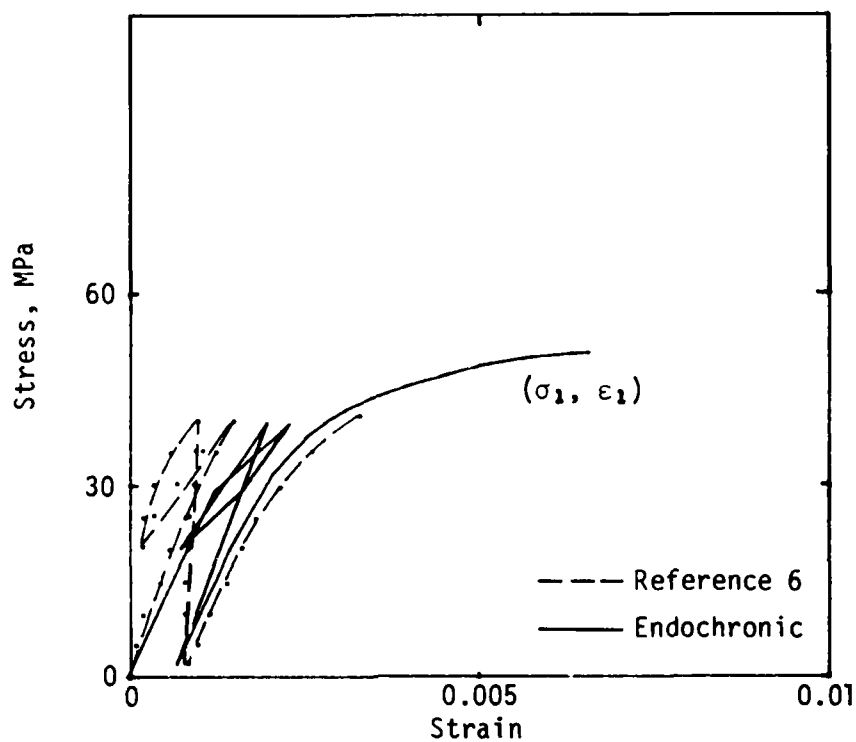


Figure 15. Stress versus strain for a loading consisting of a hydrostatic state followed by a shear cycle, and then a partial hydrostatic unload, and then an equal biaxial loading to failure.

related phenomena, such as specimen rotation, which adversely effect the accuracy of the data. Also note that the assumption of isotropic behavior in concrete is an approximation. Anisotropy had an extreme influence on several tests, particularly the equal biaxial tensile loading path. Consequently, the only loading paths discussed are those which provide clear insight into the behavior of the model.

A uniaxial tension loading path is depicted in Figure 16. It is important to emphasize that the stress and strain levels are an order of magnitude lower than those commonly occurring for compressive loads. The theoretical concrete cracking strength, defined using a standard formula (Ref. 7), gave a good representation of the strength of the material. The model predicted a stiffer response than was observed in the experiment. Anisotropic behavior appears in the experimental data for the lateral direction but is not produced in the isotropic model. Nonlinear behavior is seen in the experimental data but is not obvious in the calculated data.

A loading path consisting of a uniaxial load to $0.5 f'_t$ followed by a shear load until failure is described in Figure 17. The experimental data indicate failure at a stress slightly lower than the f'_t value. Failure for the model is defined as attainment of a stress equal to f'_t . The calculated and experimental data match well. The kink seen in plots of both sets of data occurs when the loading changes from uniaxial stress to pure shear.

Study of comparisons of predicted versus experimental data for other tensile loading paths reinforce the following observations: (1) Path dependency for the failure stress is apparent in the experimental data but is not reproducible in the model; (2) The calculated data appear to match the experimental data quite well, when test-procedure-related effects are discounted; (3) The model had a tendency to give a slightly stiffer representation of the material behavior, as was also seen in compression at low stresses.

SUMMARY

The failure points for those compressive loading paths in which failure occurred at a lode angle of either 0 deg or 60 deg are plotted in $\sqrt{J_2} - I_1$ invariant stress space in Figure 18. A linear regression fit matched the

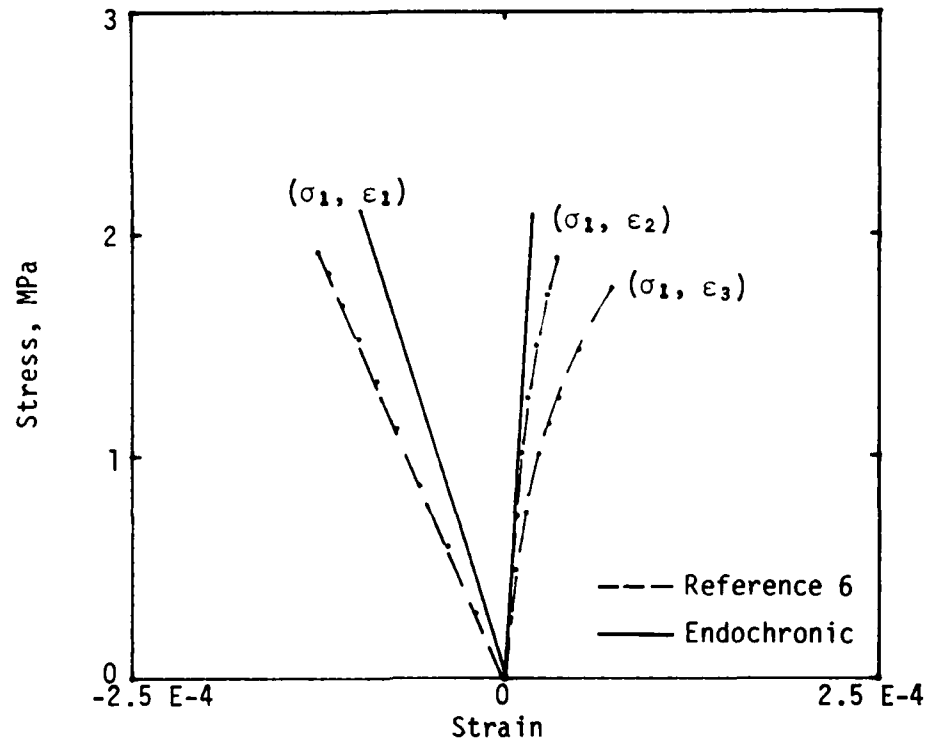


Figure 16. Stress versus strain for a uniaxial tension loading path.

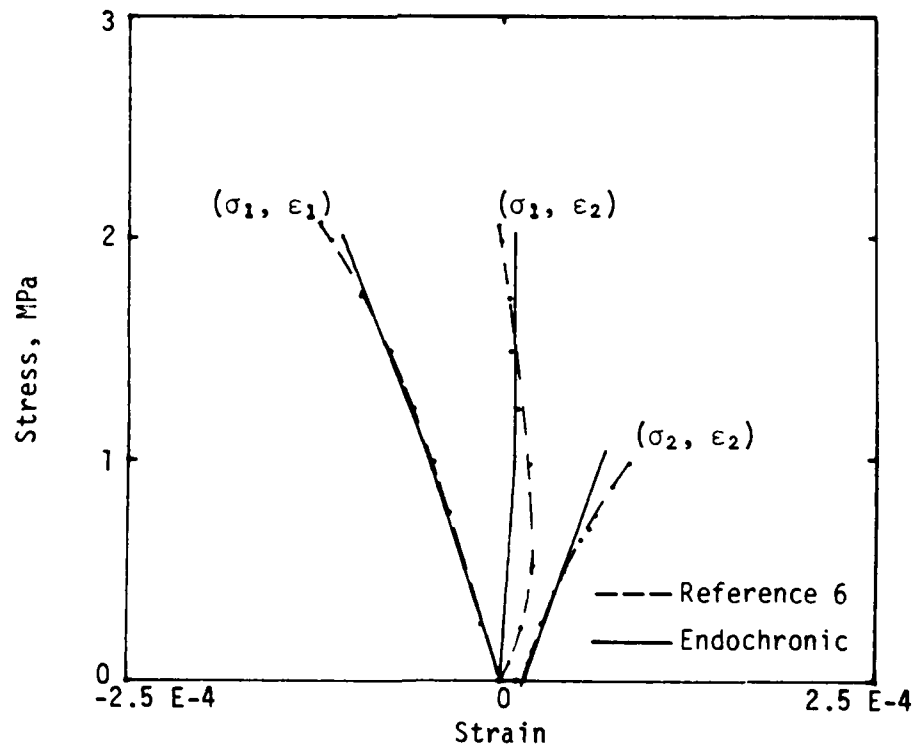


Figure 17. Stress versus strain for a shear loading superimposed on a uniaxial loading.

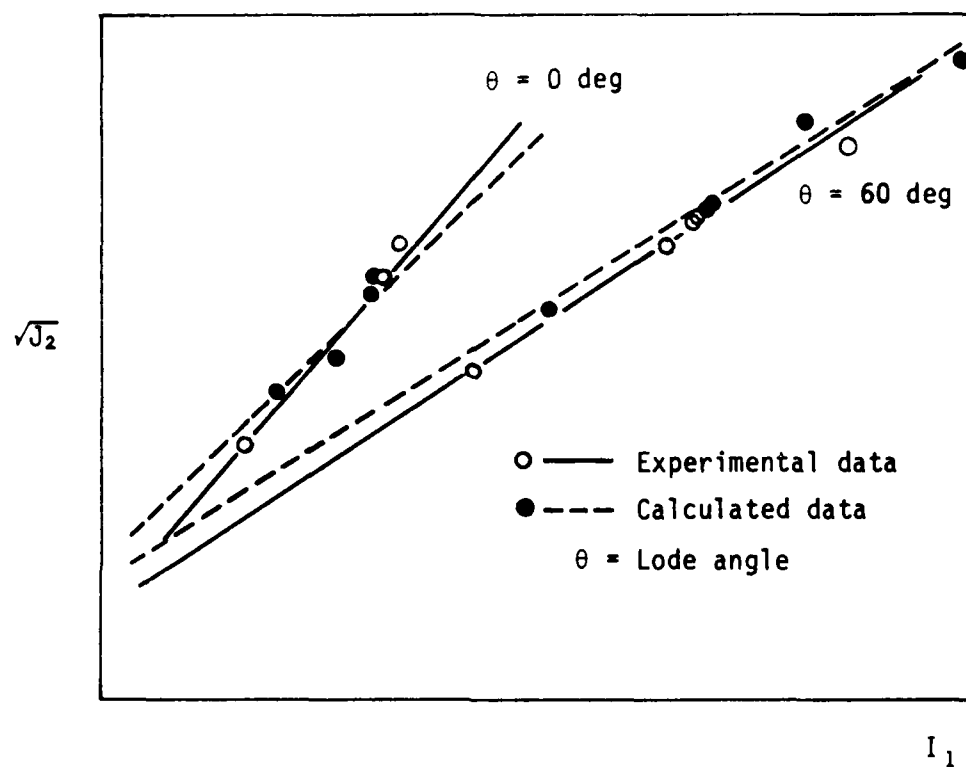


Figure 18. Calculated and experimental failure points for NMSU loading paths.

experimental and calculated data well for the load ranges considered. No attempt was made at a similar comparison for the tensile loading paths because the maximum principal stress cracking criterion does not result in a surface in this space.

When any concrete model is evaluated by comparing it with experimental data, one must consider the high degree of variation in concrete behavior caused by different aggregates, water contents, and design strengths. The method used in this study for parameter adjustment may also influence the calculated response. However, several general observations can be drawn from the comparisons of the experimental and calculated data:

1. The model provides a good qualitative match to the behavioral features observed in the material.
2. The quantitative match of the model to the experimental data varied but in general was quite good.
3. Quantitative matching of the response features suffers in certain cases when unloading-reloading cycles occur.
4. Any adjustment of the model to materials outside the range considered in fitting the initial parameters must be made with caution so that the reproduction of general stress paths is not influenced unduly.
5. Path dependence in the material is generally exaggerated in the model.

IV. GENERALIZATION OF THE ENDOCHRONIC ALGORITHM TO THREE DIMENSIONS

INTRODUCTION

A three-dimensional model was developed using the basic ideas previously incorporated for use in the endochronic constitutive model as implemented in the two-dimension finite element code SAMSON2 (Ref. 8). The resulting model can be used in two-dimensional codes by setting the appropriate shear components of the stress and strain tensor to zero.

Generalizing the two dimensional endochronic model to three dimensions involves three steps: (1) upgrading appropriate arrays and loops to the more general case; (2) choosing and implementing a three-dimensional eigenvalue-eigenvector solution technique; and (3) implementing a general second order tensor axis transformation scheme. Only the last two steps require elaboration.

DETERMINATION OF PRINCIPAL STRESSES AND DIRECTIONS

Given a state of stress at a point defined by the stress tensor \underline{g} with respect to a basis $(\underline{e}_x, \underline{e}_y, \underline{e}_z)$ there exist three mutually orthogonal planes on which the shear stresses vanish. These are the principal planes, and the normal stresses acting on these planes are the principal stresses. It is the principal stresses on which the cracking criteria are based. The problem to be solved is the eigenvalue-eigenvector problem expressed in direct tensor notation as

$$(\underline{g} - \lambda \underline{I}) \cdot \underline{\chi} = \underline{0} \quad (7)$$

where λ is an eigenvalue or principal stress and $\underline{\chi}$ is the eigenvector or principal direction associated with λ . \underline{I} is the identity tensor. For a system of linear homogeneous equations to have a nonzero solution, the determinant of the coefficients must vanish.

$$\det [\sigma_{ij} - \lambda \delta_{ij}] = 0 \quad (8)$$

where

$$\delta_{ij} = \begin{cases} i = j: \delta = 1 \\ i \neq j: \delta = 0 \end{cases}$$

The result of performing the operation defined in Equation 8 results in a cubic equation in λ which may be solved using any of a number of standard techniques. The solution method chosen here is explicit and requires no iteration. It follows the method described in Reference 9.

Expressing the determinant in terms of the deviatoric stress invariants gives

$$(\lambda')^3 - J'_2 \lambda' - J'_3 = 0 \quad (9)$$

where

$\lambda' =$ any one of the principal deviator stresses

$$\text{i.e., } \lambda'_1 = \lambda_1 - \frac{1}{3} \sigma_{kk}$$

with repeated index implying summation:

$J'_2 =$ second invariant of the deviatoric stress tensor

$$= \frac{1}{6} \left[(\sigma_{11} - \sigma_{22})^2 + (\sigma_{22} - \sigma_{33})^2 + (\sigma_{33} - \sigma_{11})^2 \right] \\ + \sigma_{12}^2 + \sigma_{23}^2 + \sigma_{31}^2$$

$J'_3 =$ third invariant of the deviatoric stress tensor
 $J'_3 = \det (\sigma_{ij}')$

where

$$\sigma'_{ij} = \sigma_{ij} - \frac{1}{3} \delta_{ij} \sigma_{kk}$$

Using the substitution

$$\lambda' = 2 \left(\frac{1}{3} J'_2 \right)^{1/2} \cos \alpha$$

in Equation 9 gives

$$2 \left(\frac{1}{3} J'_2 \right)^{3/2} [4 \cos^3 \alpha - 3 \cos \alpha] = J'_3 \quad (10)$$

Note that

$$4 \cos^3 \alpha - 3 \cos \alpha = \cos 3\alpha$$

Equation 10 becomes

$$\cos 3\alpha = \frac{J'_3}{2} \left(\frac{3}{J'_2} \right)^{3/2} \quad (11)$$

Let α_1 satisfy $0 < 3\alpha_1 < \pi$ in Equation 11 and note that $3\alpha_1$, $3\alpha_1 + 2\pi$, and $3\alpha_1 - 2\pi$ all have the same cosine; then the desired expression for the principal deviatoric and total stresses are obtained with

$$\sigma_i' = 2(\cos \alpha_i) \left(\frac{1}{3} J'_2 \right)^{1/2}$$

$$\sigma_i = \sigma_i' + \frac{1}{3} \sigma_{kk}$$

where

$$\alpha_1 = \frac{1}{3} \cos^{-1} \frac{J'_3}{2} \left(\frac{3}{J'_2} \right)^{3/2}$$

$$\alpha_2 = \alpha_1 + \frac{2\pi}{3}$$

$$\alpha_3 = \alpha_1 - \frac{2\pi}{3}$$

The principal directions are computed by solving for χ in Equation 7 for each computed λ and then normalizing to unit length. Note that the occurrence of principal stress of multiplicity greater than one is possible. For three equal principal stresses (hydrostatic stress state) the principal directions are set to the global (e_x, e_y, e_z) directions. For two equal principal stresses the directions associated with the two different stresses are computed and the third is computed using the cross-product rule.

TRANSFORMATION TO PRINCIPAL OR CRACKED BASIS

Once the principal stresses and directions have been computed the components of the stress and strain tensors are transformed from the global basis to the principal or cracked basis system. This is performed by the transformation

$$\sigma_{AB}^* = a_{Ai} a_{Bj} \sigma_{ij}$$

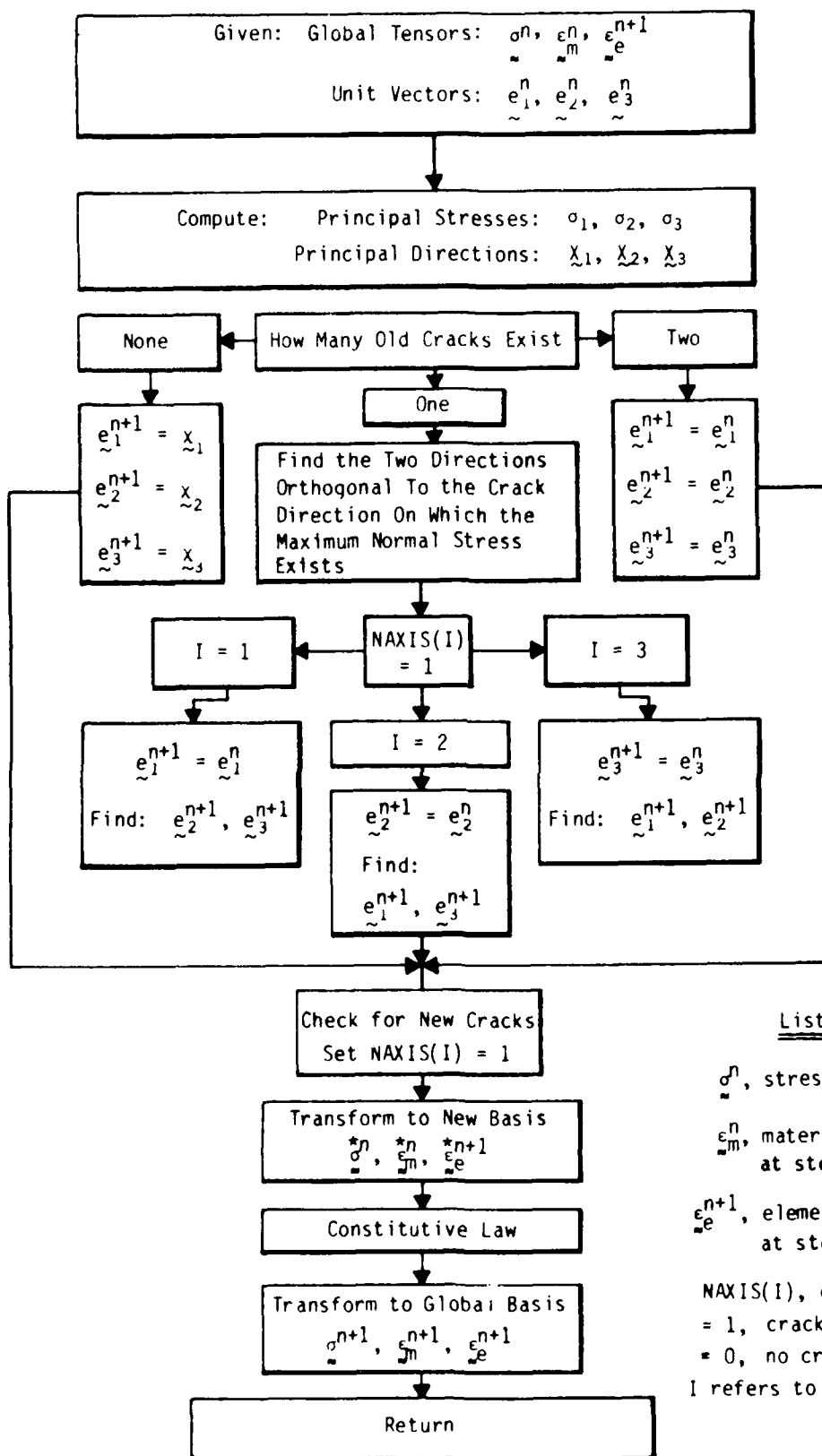
where σ_{AB}^* are the components of the tensor referred to the new basis, and a_{Ci} is the transformation matrix whose components are

$$a_{Ci} = \begin{bmatrix} e_1^1 & e_1^2 & e_1^3 \\ e_2^1 & e_2^2 & e_2^3 \\ e_3^1 & e_3^2 & e_3^3 \end{bmatrix}$$

where e_i^j is the j^{th} component of unit vector i . If these are the principal basis vectors the transformation results in a diagonal matrix whose entries are the principal stresses. Checking the principal stress against the tensile limit determines whether a crack is formed. Once a crack is noted the direction associated with the crack is recorded. When only one crack exists it is necessary to determine the other two directions orthogonal to the crack direction which reduce the shear stresses parallel to the crack plane to zero. In other words, one seeks the directions orthogonal to the crack plane on which the maximum normal stresses exist. When two cracks exist, the third direction is specified due to the assumption that cracks form orthogonal to each other.

Once the basis vectors (whether principal or crack direction) are known, the transformation is performed. Thus the constitutive model works in the principal basis when no cracks are present and in the crack direction basis if there are cracks (even when the cracks have closed). On exit from the constitutive law the inverse transformation is performed so that global stresses and strains are available for printout and other required computations.

Figure 19 is a flow chart of steps involved in the directional cracking analysis.



List of Symbols

$\underline{\sigma}^n$, stress tensor at step n

$\underline{\epsilon}_m^n$, material strain tensor at step n

$\underline{\epsilon}_e^{n+1}$, element strain tensor at step n+1

$NAXIS(I)$, crack indicator
= 1, crack in I direction
= 0, no crack in I direction
I refers to unit vector \underline{e}_I

Figure 19. Flow chart of the directional cracking model.

V. HIGH STRAIN RATE EFFECTS IN THE ENDOCHRONIC CONCRETE MODEL

INTRODUCTION

The impulse loads considered for the analysis of protective structures are of such a magnitude that significant strain rate effects are expected in the material response. This effect influences the structural response through a strength enhancement effect at high strain rates and through resulting effects on stress distribution and redistribution in indeterminate structures. Existing concrete models either ignore these effects or treat them in an artificial fashion. In this section a modified version of the endochronic concrete model which deals with strain rate effects is described. This approach is simple and flexible, but is in a form which appears compatible with the physical phenomena involved.

REVIEW OF CONCRETE STRAIN RATE EFFECTS

The current state of knowledge in the area of strain rate effects on the compressive behavior of concrete is summarized in recent reports by Bazant and Oh (Ref. 10) and Suaris and Shah (Ref. 11). A study of these summaries and other specific reports on experimental studies (Refs. 12 and 13) reveals two interesting points about the current perception on strain rate effects on concrete. First, most of the existing experimental data are concerned with testing under nominally uniaxial stress conditions. Second, strains are often measured in an indirect fashion which creates some question about any conclusion about performance at a given strain rate. Despite the nebulous nature of the existing data, some conclusions are currently accepted with regard to high strain rate effects. It appears that, with an increase in strain rate, the extent of internal microcracking decreases, resulting in less nonlinearity in the stress-strain relations at high strain rates. The result is an increase in strength, secant modulus, and strain at failure for the concrete. Although these conclusions are primarily based on uniaxial stress conditions, similar results were seen in the limited amount of multiaxial data available.

ENDOCHRONIC APPROACH TO HIGH STRAIN RATE EFFECTS IN CONCRETE

Although strain rate effects were considered in the earlier development of the endochronic concrete theory described in Reference 2, the concern was creep rather than high strain rate effects. An endochronic approach has been applied to metals subjected to a constant strain rate by Lin and Wu (Ref. 14), who later developed a formulation applicable to variable strain rates in metals (Ref. 15). This work serves to indicate the potential of the endochronic model for representing strain rate effects. Specifically, the intrinsic time term provides an attractive avenue for inclusion of strain rate effects.

Consider a heuristic example: A representative intrinsic time increment term could be of the form

$$d\zeta = F_1(\sigma, \epsilon)(de_{km}de_{km})^{1/2}$$

or, alternately

$$d\zeta = F_1(\sigma, \epsilon)(\dot{e}_{km}\dot{e}_{km})^{1/2} dt$$

where

($\dot{}$) indicates differentiation with respect to time.

Neither of the above expressions has a rate dependency. However, a variation of the form

$$d\zeta = F_1(\sigma, \epsilon)(\dot{e}_{km}\dot{e}_{km} + C)^{1/2} dt$$

would have a rate dependency. The C term could represent a constant or a function. The intrinsic time increment term could be rewritten as

$$d\zeta = F_1(\sigma, \epsilon) \left[1 + \frac{C}{\dot{e}_{km}\dot{e}_{km}} \right]^{1/2} (de_{km}de_{km})^{1/2}$$

which is the same as the first expression considered, except for the bracketed term, which introduces strain rate effects. For this simple model it is seen that low strain rates produce larger intrinsic time increment terms than

high strain rates. Since the intrinsic time term serves as a measure of damage (microcracking) in the concrete, an adjustment of this form can be related to the decrease in internal microcracking hypothesized from experimental data. The reduction of the intrinsic time increment in the model reduces the inelastic portion of the material response, resulting in a strengthening of the material.

Since different intrinsic time terms are used in the endochronic concrete model for plastic and fracturing deviatoric behavior and for some inelastic volumetric behavior, different strain rate considerations could be made for these different phenomena. The need for such considerations was investigated using data from uniaxial testing with the corresponding average strain rate taken as constant. Applying the high strain rate modification only to the intrinsic time term related to plastic deviatoric behavior produced the most satisfactory results. Consequently, the formulation described in this section is constrained in that fashion. Subsequent availability of more detailed experimental data may require an adjustment to this approach.

The simple formulation described above is unsuitable for general use if C is a constant, but serves to indicate the ability of the theory to accommodate strain rate effects. A more appropriate expression could be determined by choosing the C -term to be a function. A convenient alternative is to replace the entire bracketed term with a term consistent with observed high strain rate behavior. A suitable starting point is a modification of an expression used for metals for a similar purpose in Reference 15:

$$d\zeta = k(de_{km}de_{km})^{1/2}$$

where

$$k = 1 - k_a \log \frac{\dot{e}_{km}}{\dot{e}_0} - k_b \left[\log \frac{\dot{e}_{km}}{\dot{e}_0} \right]^2$$

and

k_a , k_b , \dot{e}_0 are parameters to be determined

The influence of different k values on the response of the endochronic model is described in Figure 20 for uniaxial stress loadings. Increased strength, secant modulus, and strain at failure are all reflected in the behavior of the model.

In evaluating the validity of the expression given above for k , as in determining appropriate parameters for the expression, one is limited by the sparsity of experimental data. Operating, once again, within the constraint of uniaxial stress data and utilizing the average strain rate as if it were constant, one can define appropriate values for the k_a , k_b , and $\dot{\epsilon}_0$ parameters by using summary data such as that presented in Figure 21 (Ref. 11). The resulting parameters are not unique but appear to produce reasonable results. They are

$$k_a = 0.09$$

$$k_b = 0.0015$$

$$\dot{\epsilon}_0 = 0.5 \text{ E-5}$$

SUMMARY

Concrete strain rate effects are reviewed in this section and a modification to the endochronic concrete model to reflect these effects is proposed. The modification ties strain rate effects into the portion of the model which deals with the physical phenomena considered to cause such effects.

The resulting model is not appreciably more complicated than the time-independent endochronic model and is amenable to change if such change appears warranted by advances in knowledge of strain rate effects. A detailed check-out of the model through comparison with existing multidimensional test data is desirable.

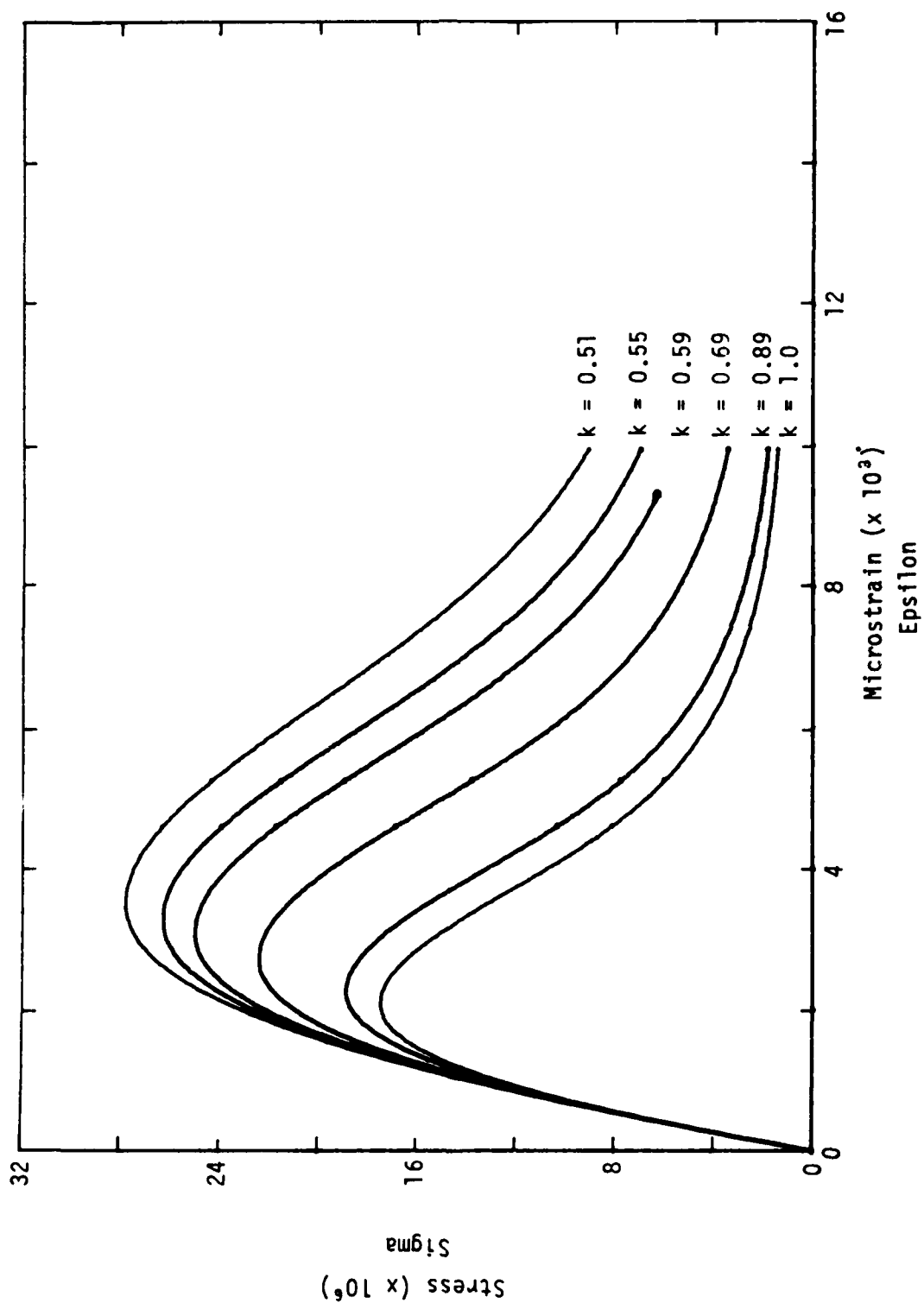


Figure 20. Effect of k parameter on the response of the endochronic concrete model for constant strain rates.

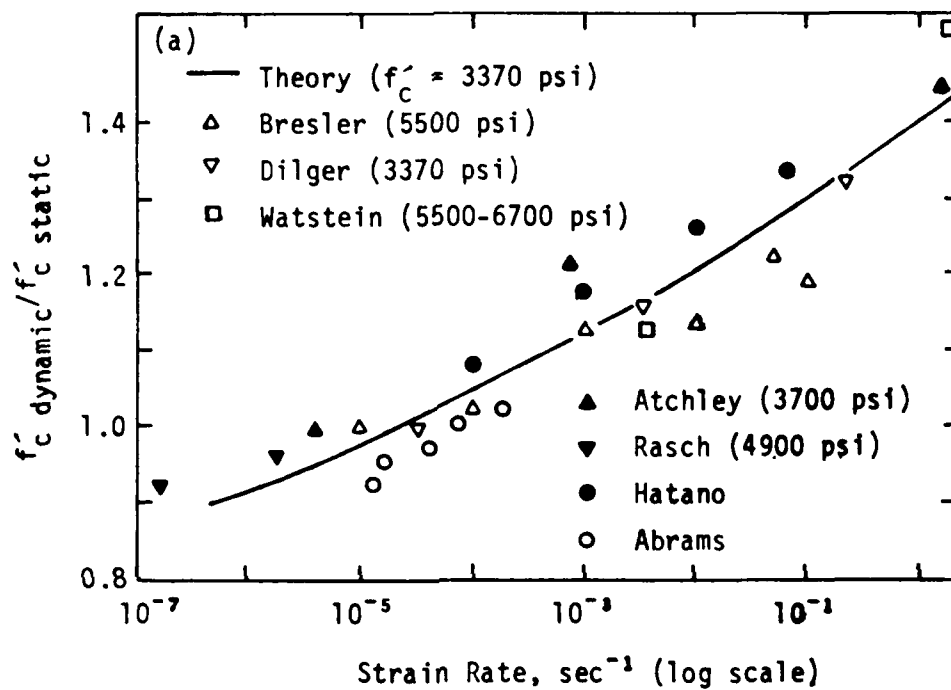


Figure 21. Effect of strain rate on concrete strength (from Ref. 11).

VI. REDUCTION OF STORAGE REQUIREMENTS

INTRODUCTION

The present form of the endochronic algorithm requires that 27 parameters be stored per element for each load/time step. Storage requirements of this magnitude are commonly required for models which include hysteresis effects. Indeed, elimination of the hysteresis-related stored parameters would leave only 10 stored parameters for the combined endochronic and crack-ing model. Nevertheless, the capability of the model as an effective analysis tool is inhibited by excessive storage requirements. Although inclusion of hysteresis effects makes the algorithm more rigorous, such rigor may be necessary only when the model is used as a research tool or for problems involving significant cycling. Consequently, simplification of the approach used for cyclic loading is an appropriate consideration for attaining a reduction in the storage requirements for the model.

ALTERNATE SCHEMES FOR HYSTERESIS

The approach currently used for hysteresis requires 6 storage elements to define the loading states of unloading/reloading/virgin loading, 2 storage elements for adjustments to the equations based on the loading state, and 9 storage elements to describe jump-kinematic hardening. Three alternate schemes were considered for simplifying the model. The first was complete elimination of specific hysteresis modeling within the algorithm. This approach eliminates the 17 storage parameters related to hysteresis, but would produce unadjusted endochronic unloading and reloading, a condition which implied the creation of energy in earlier endochronic models. Excessive accumulation of the deviatoric strain path length would also be expected to occur under cyclic loading, resulting in an artificial hardening of the material.

The second scheme considered was intended to be a compromise between the total elimination of hysteresis and the existing model. In this version the adjustment which prevented excessive accumulation of the deviatoric strain path length was retained from the original model. It is necessary to differentiate between virgin/renewed-virgin loading and unloading/reloading for this approach. The number of storage parameters related to hysteresis is reduced to 6.

The third approach which was studied used an elastic description for unloading and reloading. A means of differentiating between virgin/renewed virgin loading and unloading/reloading is again necessary. The endochronic portion of the algorithm is bypassed during unloading and reloading, so no incremental inelastic behavior is produced. A modest increase in efficiency would be expected as a consequence. This scheme results in a reduction to 4 of the number of storage parameters related to hysteresis.

EVALUATION OF ALTERNATE SCHEMES

Evaluation of alternatives to the complete hysteresis model presently in the model was done by considering only uniaxial loading paths, since most of the available data on hysteretic behavior fall into this category. Behavior for multidimensional loadings can be extrapolated for each scheme, to some degree, from the uniaxial paths.

One loading path considered was a cyclic loading consisting of complete unloading/complete reloading cycles. This is a duplication of a path for which experimental data are available (Ref. 16). The matchup to these data for the complete hysteresis model is shown in Figure 22. The model produces hysteresis, follows the general envelope of the experimental data, and reflects the degradation of the elastic modulus.

Results for the alternate scheme in which hysteresis modeling was eliminated are compared to the experimental results in Figure 23. Hysteresis is eliminated; in fact, Drucker's postulate is violated. Degradation of the elastic modulus is seen to occur. The model appears to produce a reasonable depiction of the envelope of the experimental data, although it overshoots the envelope in the high strain range.

Some insight into the behavior described above can be found by studying Figure 24 which compares the same experimental results with results from the second approximate scheme. This approach included the adjustment which prevented excessive accumulation of the deviatoric strain path length. Since it has been shown that the excessive accumulation of the deviatoric strain path length results in hardening, it was expected that elimination of this accumulation would result in a somewhat softer response; however, the extreme softening requires an explanation.

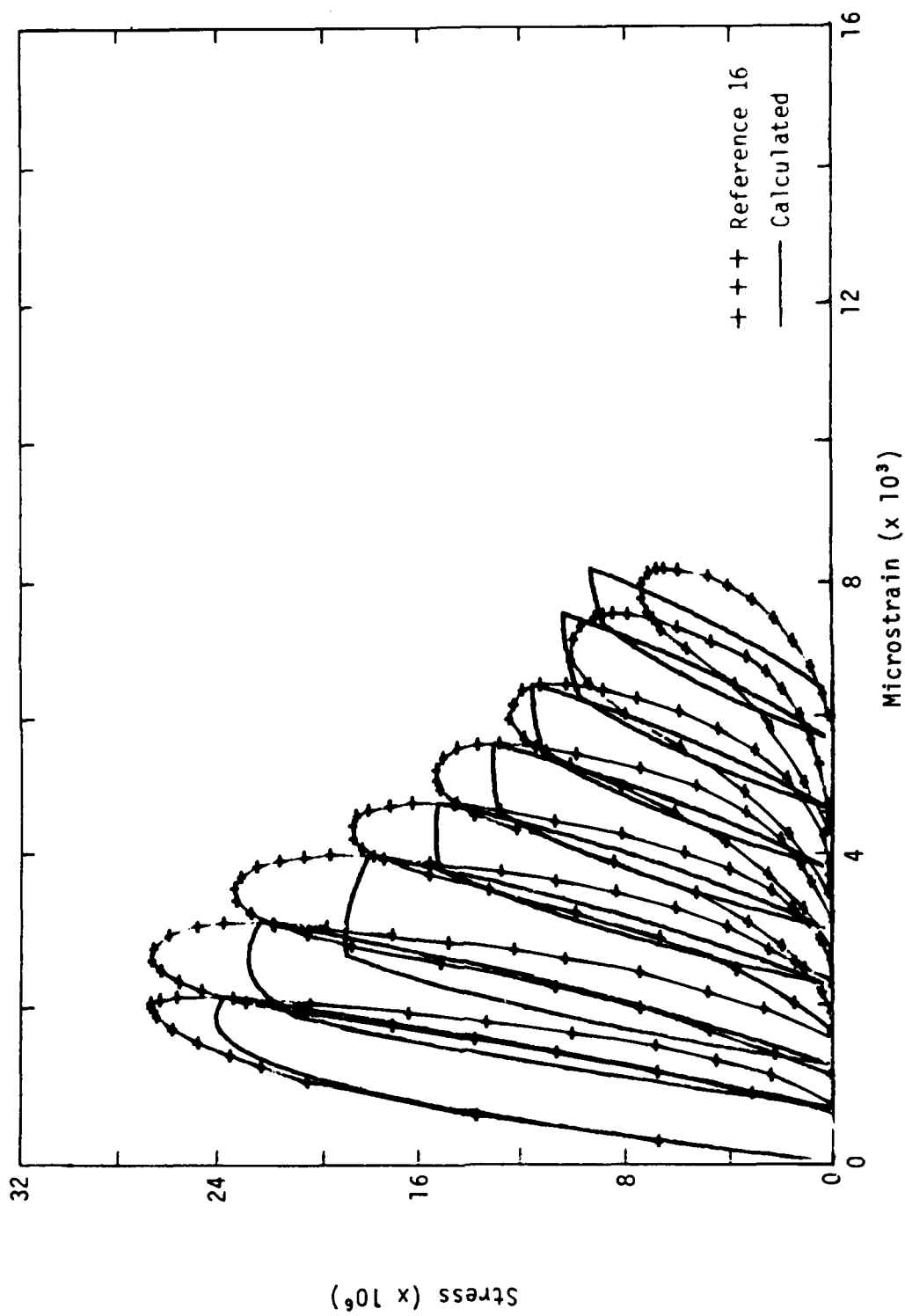


Figure 22. Stress versus strain for uniaxial cyclic compression using the original hydrostatic endochronic algorithm.

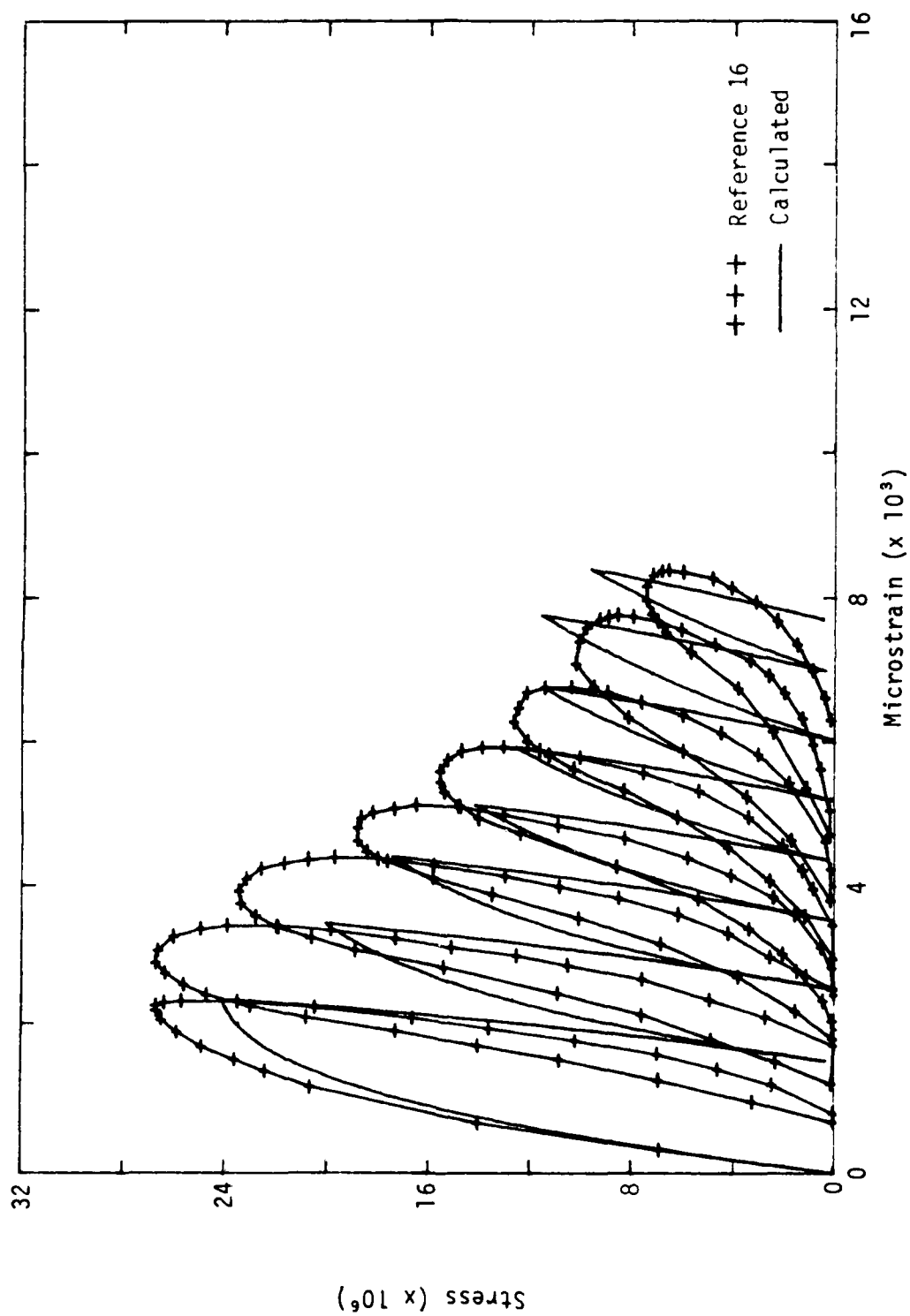
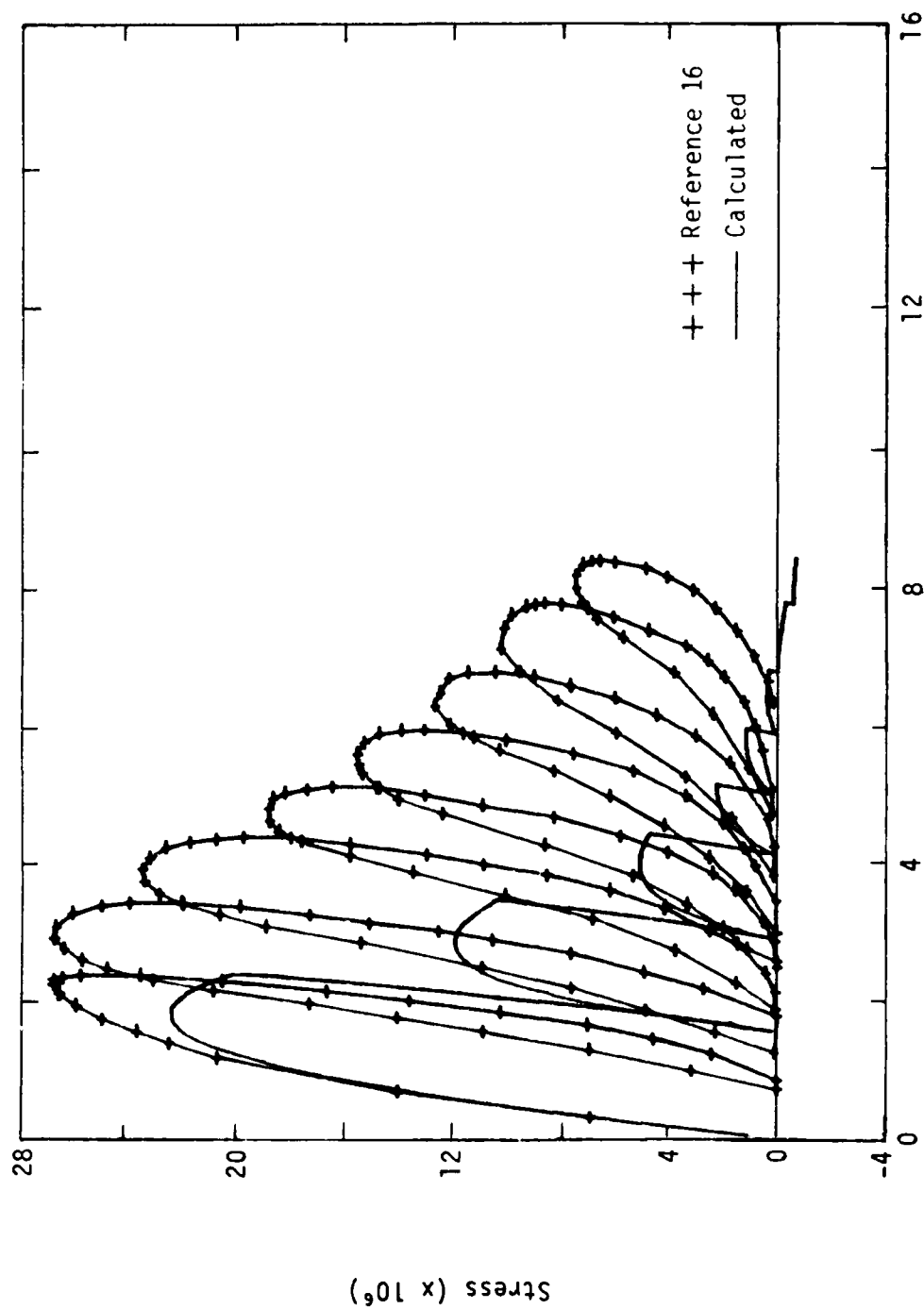


Figure 23. Stress versus strain for uniaxial cyclic compression using the endochronic algorithm without hysteretic consideration.



Microstrain ($\times 10^3$)

Figure 24. Stress versus strain for uniaxial cyclic compression using the modified hysteretic endochronic algorithm.

The problem considered was cycled by loading to a given strain, and then unloading to a zero stress. In the original model the stiffness associated with reloading is lost when virgin loading is renewed for two reasons: (1) the center for jump-kinematic hardening is redefined (not applicable in this case), and (2) adjustments to the formulation are made, in particular, the deviatoric strain path length is reset. Renewed virgin loading is defined to occur when the deviatoric strain energy lost in the unloading process is restored. When the hysteresis model is completely eliminated, one would expect softer behavior, since the strain at which the next unload cycle should occur would be reached at a lower stress level without the influence of hysteresis. The reason the first scheme, which excluded special consideration for unloading, did not appear softer is because excessive accumulation of the deviatoric strain path length produced a compensating hardening effect. The modified version which did not allow such excessive accumulation produced a much softer and unacceptable response. Since the interaction of these two effects in the first scheme cannot be expected to be so accommodating for general loading conditions, one must suspect that the first scheme may also be undesirable as a simplifying approximation. It should be emphasized, however, that either scheme could be suitable for a loading which is known to be free of significant unloading.

The third approach considered, which utilized an elastic scheme for unloading and reloading, is compared with the experimental data in Figure 25. Degradation of the elastic modulus can be seen, but hysteresis is not represented. The envelope of the experimental data is violated because renewed virgin loading is defined at a higher stress than for the other schemes due to the elastic behavior during the cycle.

Generally, a simplified version of the hysteresis modeling would be utilized for problems where hysteresis would not be expected to have a significant influence. However, there is evidence that the hysteresis model is a sensitive aspect of the overall endochronic formulation. For instance, the modification described in Section I of this report resulted from a slight fault in the jump-kinematic hardening model which produced an inordinant amount of hardening. This behavior is displayed in Figure 26, where a virgin

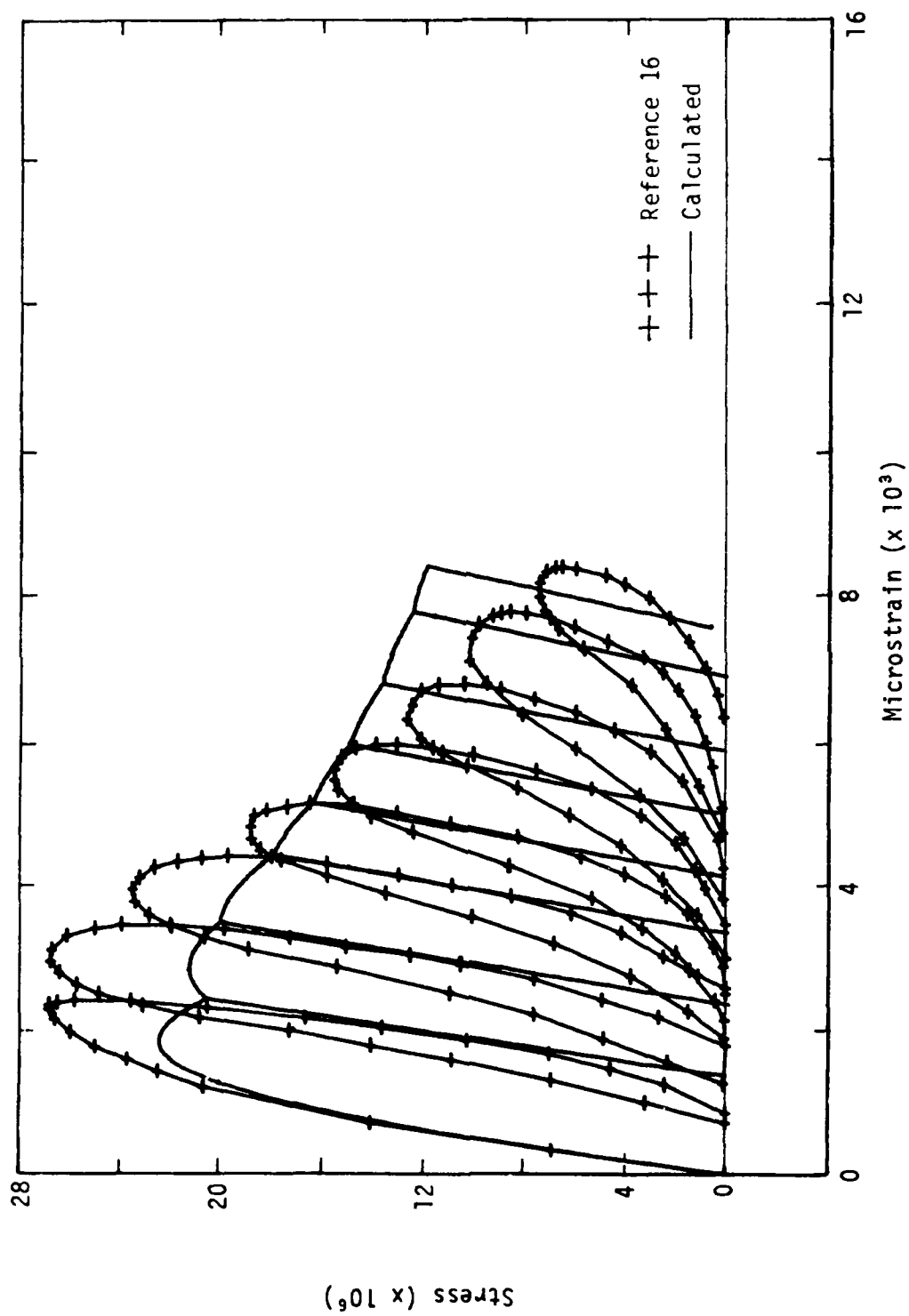


Figure 25. Stress versus strain for uniaxial cyclic compression using the endochronic algorithm with elastic cycling.

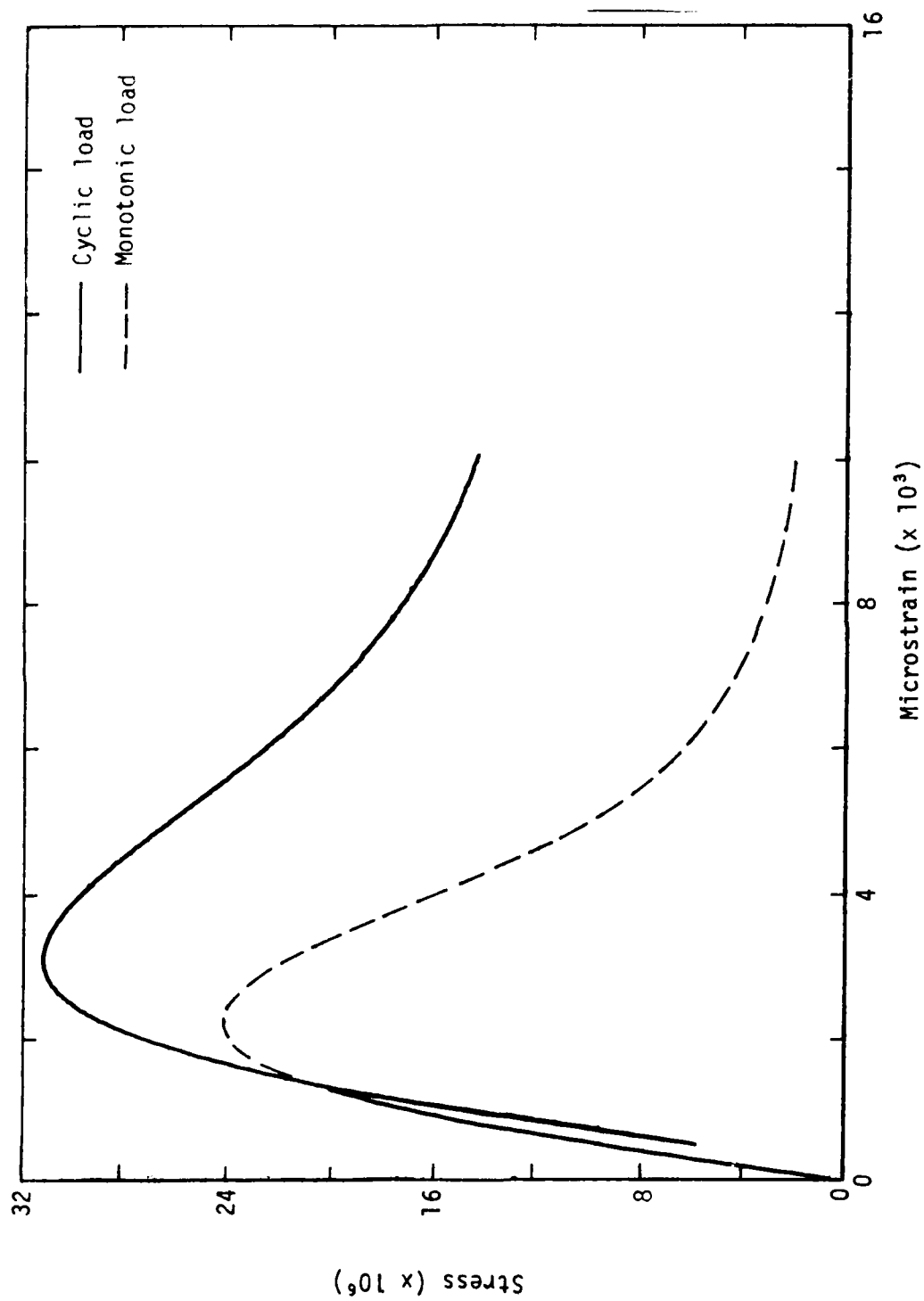


Figure 26. Stress versus strain for uniaxial compression with a single partial unloading cycle using the uncorrected jump-kinematic hardening representation.

loading curve is compared to a similar loading which included a small unload-reload cycle. A similar comparison is made in Figure 27, where the modified version of the model is used. Factors such as the virgin loading definition still have some influence on the results, but the representation is acceptable. It is important to note that behavior such as this is not uncommon for concrete, where a loading redistribution due to cracking or strain softening could result in a slight unloading at a point in the material. The first and third schemes were studied under this type of load. In Figure 28 the virgin loading curve is superposed in the results of the first scheme, which eliminated hysteresis considerations, for the load which included the small cycle. The energy stored in this model is exaggerated compared to the virgin loading. This excess is due to accumulation of the deviatoric strain path length during the cycle. A much more acceptable comparison is seen in Figure 29, where the scheme with the elastic unloading is considered.

Another concern with simplified approaches to hysteresis is whether the model is consistent with the virgin loading curve as an envelope during multiple cycles. Figure 30 compares this envelope with the existing model. Some violation of the envelope is seen to occur. The loading is repeated in Figure 31 for the alternate scheme which ignores hysteresis. The effect of an accumulation of the intrinsic time term is obvious in the extreme violation of the envelope. Similar comparisons are made in Figure 32 for the scheme which unloaded/reloaded elastically. This comparison is severely affected by the loading technique. The loadings were applied until a given strain was reached, while the unloading was stopped at a given stress. Thus, the results were affected by the lack of hysteresis representation in the model. A similar misrepresentation could occur for a general loading. Note that similar problems would exist for any model that unloads and reloads elastically.

SUMMARY

Any of the alternate versions of the endochronic model will give reasonable results if no hysteresis is present. The scheme in which hysteresis considerations were eliminated tends to produce exaggerated hardness in the presence of cycling. The balance between softness due to endochronic unloading and hardness due to accumulation of deviatoric strain path length, which

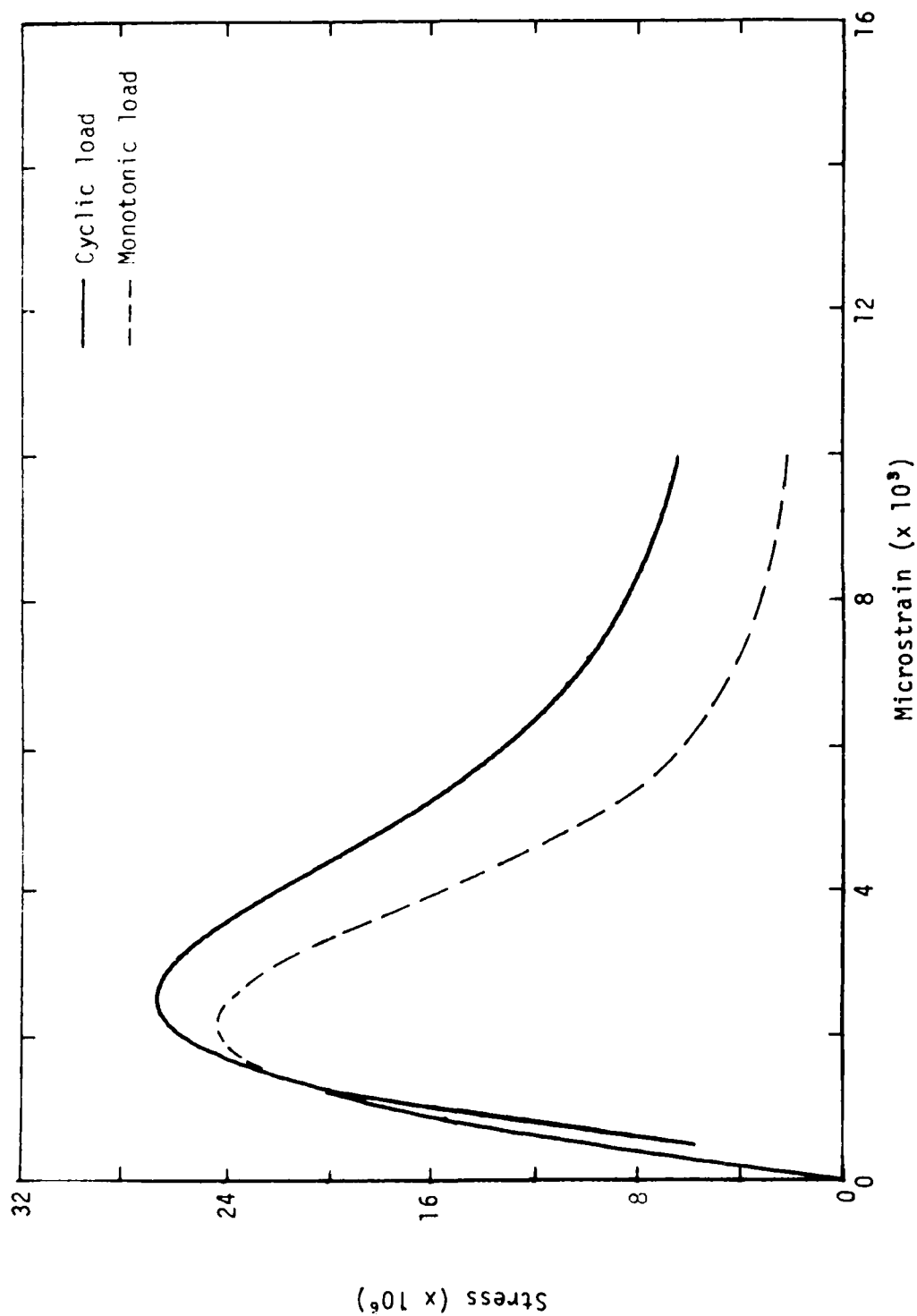


Figure 27. Stress versus strain for uniaxial compression with a single partial unloading cycle using the modified jump-kinematic hardening representation.

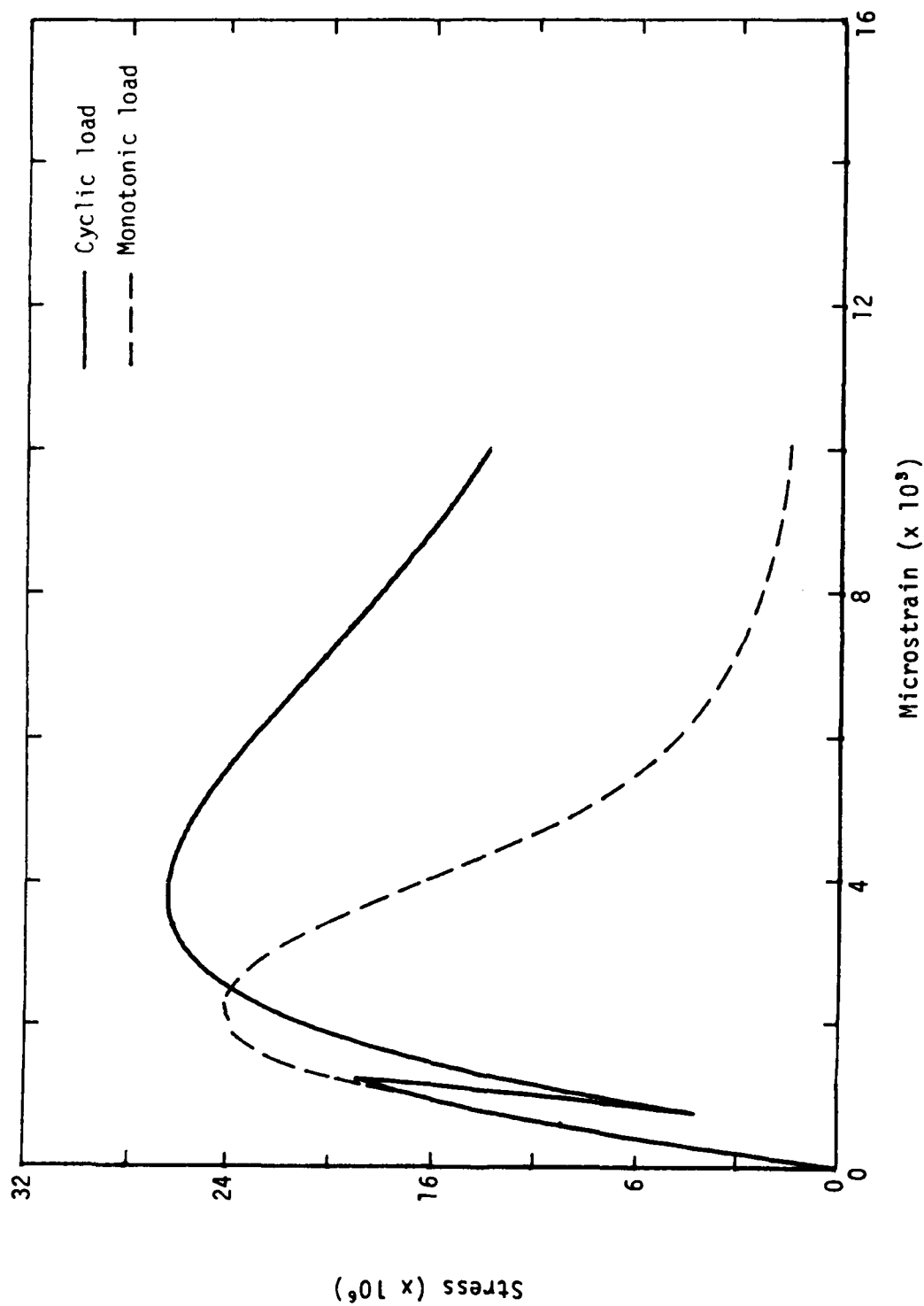


Figure 28. Stress versus strain for uniaxial compression with a single partial unloading cycle for the endochronic algorithm without hysteretic considerations.

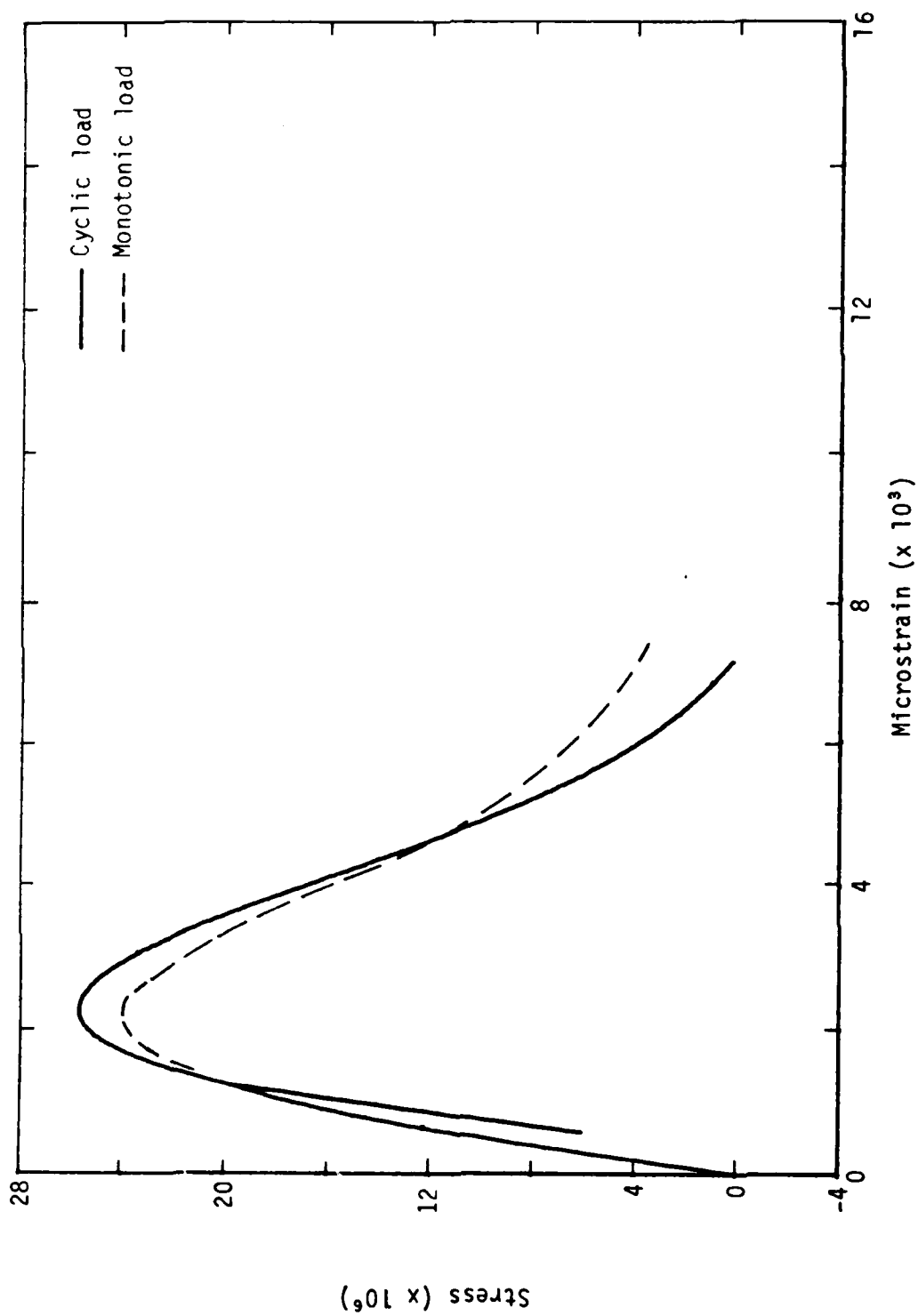


Figure 29. Stress versus strain for uniaxial compression with a single partial unloading cycle for the endochronic algorithm with elastic cycling.

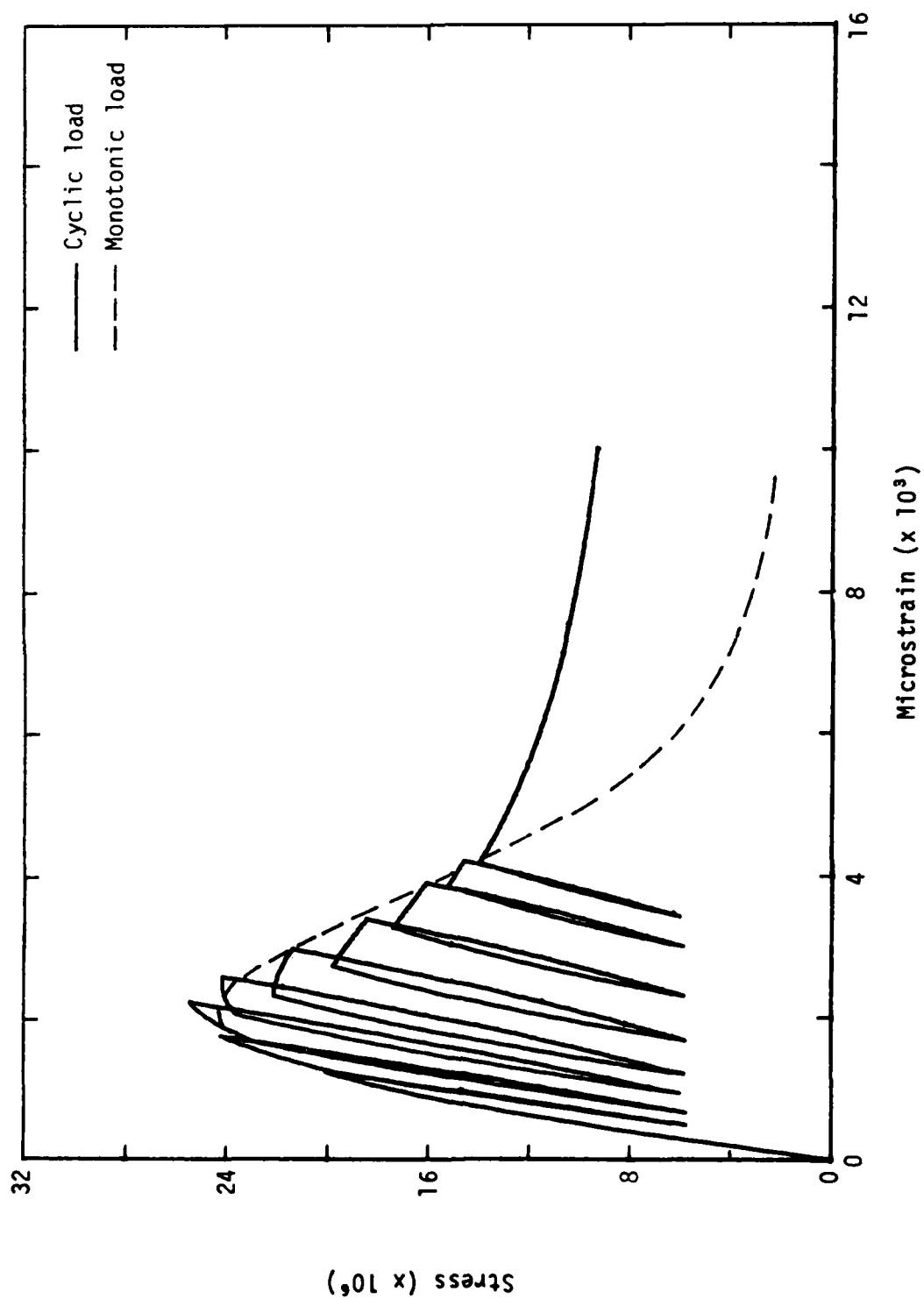


Figure 30. Stress versus strain for uniaxial compression with multiple cycling using the original endochronic algorithm.

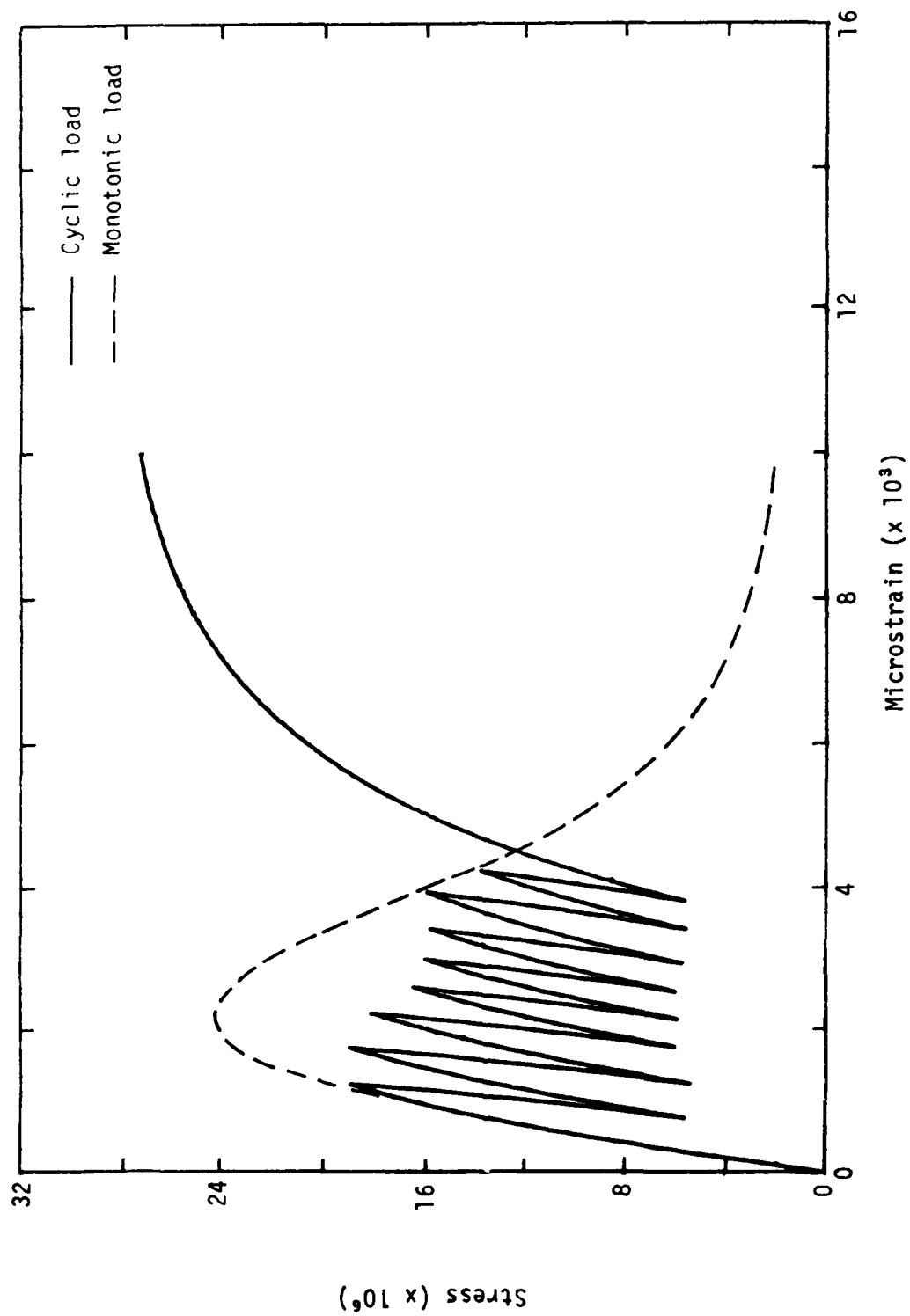


Figure 31. Stress versus strain for uniaxial compression with multiple cycling using the endochronic algorithm without hysteretic considerations.

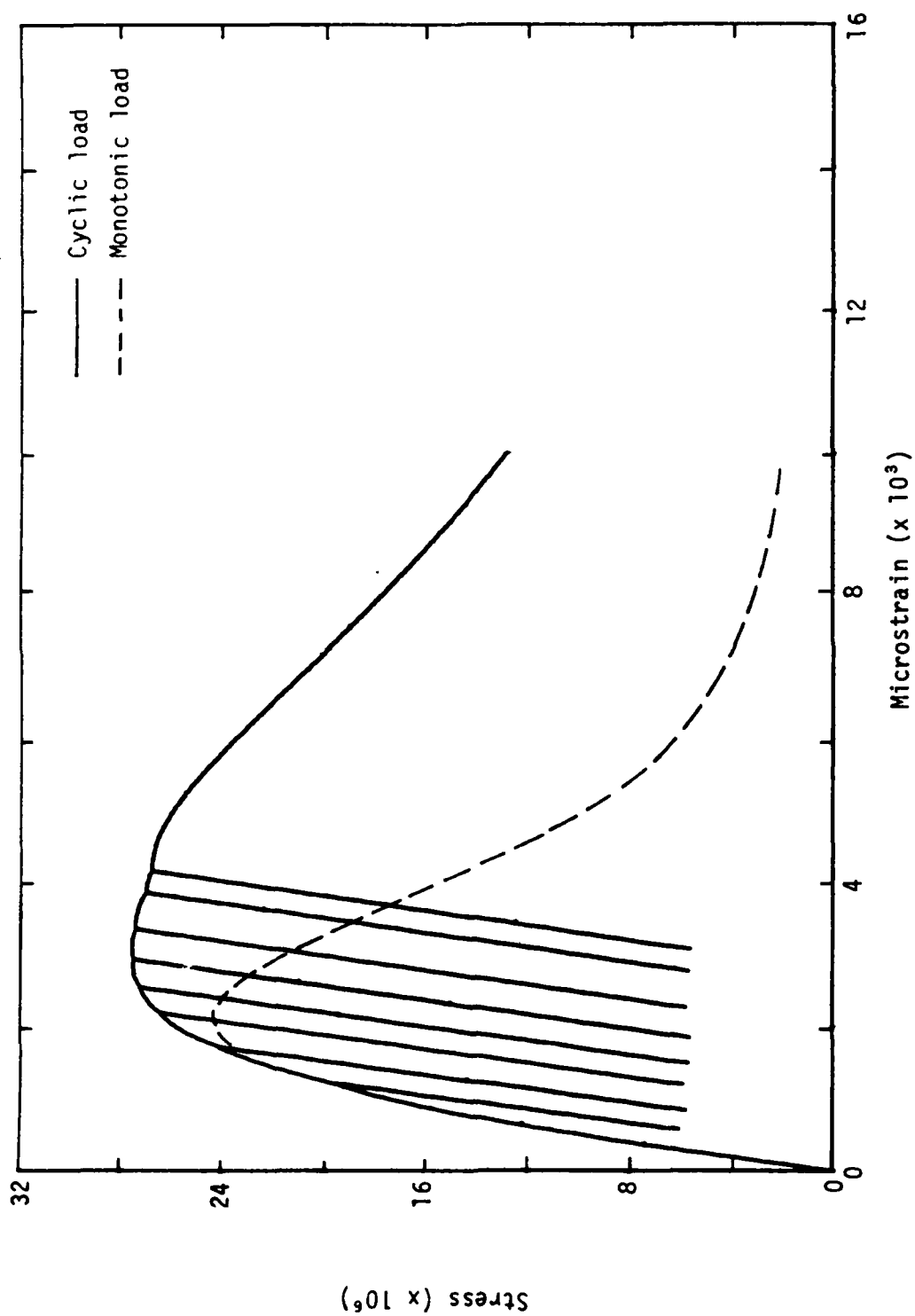


Figure 32. Stress versus strain for uniaxial compression with multiple cycling using the endochronic algorithm with elastic cycling.

was seen for the uniaxial cyclic loading, should not be expected to exist for general loads. The approach which adjusted for the accumulation of deviatoric strain path length responded much too softly in the presence of unloading. The scheme which defined unloading and reloading elastically appeared to give the most reasonable results.

VII. CONCLUSIONS AND RECOMMENDATIONS

CONCLUSIONS

The endochronic concrete algorithm as considered in this study continues to gain credibility as a viable concrete model. It demonstrates a capability of reflecting all significant behavioral characteristics of concrete under static loading and has shown the flexibility required for the incorporation of dynamic effects. Conclusions derived from this effort are

1. The model provides a good qualitative match to the behavioral features observed in the material for a variety of loading paths. This performance lends credence to the ability of the model to handle general loading paths.
2. The model fares worst under circumstances for which the intrinsic time term accumulates excessively. This was particularly evident for loadings which paralleled the failure surface.
3. Adjustment of the model to concretes outside the range considered in calibrating the original model should be done with caution to avoid unduly influencing the reproduction of general stress paths.
4. The most promising approach to parameter reduction is the scheme which defines unloading and reloading elastically. This reduces the number of parameters related to hysteresis to 6, so the total number of stored parameter for the directional cracking/endochronic compression model is 16.

RECOMMENDATIONS

This investigation has shed considerable light on the potential of the endochronic concrete model as a practical analytical tool. However, several areas have been uncovered which require investigation. Consequently, it is recommended that consideration be given to the following areas for further study:

1. There is some discrepancy between the model and the relatively meager data available for loading paths parallel or nearly parallel to the

failure surface. It is recommended that the model be tested against data recently generated at the University of Colorado which studies these loadings in some detail.

2. A problem seen in matching some of the NMSU stress paths was the excessive accumulation of the intrinsic time increment. The excessive accumulation was often associated with stress paths which involved some cyclic behavior. It is recommended that a detailed study be made of the influence of the load-unload criteria on the behavior of the model. Alternate criteria would be a consideration.

3. The initial approach to strain rate effects made in this study for the endochronic model proves to be quite promising, based on comparison with the limited amount of one-dimensional data. Comparisons with the limited amount of multidimensional data are now desirable, followed by interaction between the model and a strong experimental program.

4. The parameter reduction investigation was done without permanently changing the endochronic model coding. The change should be made permanent through appropriate changes in the code. This would result in a separate code for use when hysteresis effects are not needed in the model.

5. At this point, consideration should be made to expansion of the model to include the effects of reinforcing steel. This would make the model more efficient and, ultimately, more accurate as more aspects of reinforced concrete behavior are introduced. This problem could be approached in three stages. The first stage involves a simple smearing of the reinforced steel; the second would introduce aspects of steel concrete interaction; and the third phase would be an investigation of an anisotropic model which could handle the effect of the steel as efficiently as possible.

REFERENCES

1. Bazant, Z. P., and Schieh, C. L., "Hysteretic Fracturing Endochronic Theory for Concrete," Journal of the Engineering Mechanics Division, American Society of Civil Engineers, Vol. 106, No. EM5, Proceedings Paper 15781, pp. 929-950, October 1980.
2. Bazant, Z. P., and Bhat, P., "Endochronic Theory of Inelasticity and Failure of Concrete," Journal of the Engineering Mechanics Division, American Society of Civil Engineers, Vol. 102, No. EM4, Proceedings Paper 12360, pp. 701-722, August 1976.
3. Bazant, Z. P., and Kim, S. S., "Plastic-Fracturing Theory for Concrete," Journal of the Engineering Mechanics Division, American Society of Civil Engineers, Vol. 105, No. EM3, pp. 407-428, June 1979.
4. Schreyer, H. L., and Jeter, J. W., Reinforced Concrete Modeling, AFWL-TR-82-9, Air Force Weapons Laboratory, Kirtland Air Force Base, New Mexico, February 1982.
5. Bazant, Z. P., "Endochronic Inelasticity and Incremental Plasticity," International Journal of Solids and Structures, Vol. 14, No. 9, pp. 691-714, September 1978.
6. Traina, L. A., Experimental Stress-Strain Behavior of a Low-Strength Concrete under Multiaxial States of Stress, AFWL-TR-82-92, Air Force Weapons Laboratory, Kirtland Air Force Base, New Mexico, May 1982.
7. Building Code Requirements for Reinforced Concrete, ACI 318-77, American Concrete Institute, Detroit, Michigan, October 1977.
8. Belytschko, T., and Robinson, R. R., SAMSON2: A Nonlinear Two-Dimensional Structure/Media Interaction Computer Code, AFWL-TR-81-109, Air Force Weapons Laboratory, Kirtland Air Force Base, New Mexico, January 1982.
9. Malvern, L. E. Introduction to the Mechanics of a Continuous Medium, Prentice-Hall, Englewood Cliffs, New Jersey, 1969.
10. Bazant, Z. P., and Oh, B. H., "Strain Rate Effect in Rapid Nonlinear Tri-axial Deformation of Concrete," Journal of the Engineering Mechanics Division, American Society of Civil Engineers, Vol. 108, No. EM5, pp. 764-782, October 1982.
11. Suaris, W., and Shah, S. P., "Mechanical Properties of Materials Sub-jected To Impact," Introductory Report, Symposium on Concrete Structures Under Impact and Impulse Loading, Bundesanstalt fur Materialprufing (BAM), Berlin, June 4, 1982.

12. Watstein, D., "Effect of the Straining Rate on the Compressive Strength and Elastic Properties of Concrete," ACI Journal, Vol. 49, No. 8, pp. 729-744, April 1953.
13. Atchley, B. L., and Furr, H. L., "Strength and Energy Absorption Capabilities of Plain Concrete Under Dynamic and Static Loading," ACI Journal, pp. 745-756, November 1967.
14. Lin, H. C., and Wu, H. C., "Strain Rate Effect in the Endochronic Theory of Viscoplasticity," Journal of Applied Mechanics, pp. 92-96, March 1976.
15. Lin, H. C., and Wu, H. C., On the Improved Endochronic Theory of Viscoplasticity and Its Application to Plastic Wave Propagation, ANL-CT-81-37, Argonne National Laboratory, Argonne, Illinois, October 1981.
16. Sinha, B. P., Gerstle, K. H., and Tulin, L. G., "Stress-Strain Relations for Concrete under Cyclic Loading," Journal of the American Concrete Institute, Vol. 61, No. 2, pp. 195-210, February 1964.

END

FILMED

7-83

DTIC